The 14-3-3/spastin pathway coordinates neurite regeneration and recovery of spinal cord injury by targeting microtubule dynamics

Author: Qiuling Liu[1#], Hua Yang[1#], Jianxian Luo[1#], Cheng Peng[1], Ke Wang[1], Guowei Zhang[1], Zhisheng Ji[1]*, Hongsheng Lin[1]*

1 Department of Orthopedics, The First Affiliated Hospital of Jinan University, Guangdong province, Guangzhou 510630, People's Republic of China;

[#]These authors contribute equally to this work.

*** Corresponding to:**

Zhisheng Ji (jizhisheng0521@163.com)

Hongsheng Lin (tlinhsh@jnu.edu.cn)

Department of Orthopedics, The First Affiliated Hospital of Jinan University, 613 Huangpu Avenue, Guangzhou 510630, People's Republic of China.

Running title: 14-3-3/spastin pathway regulates the recovery of spinal cord injury.

Abstract Axon regeneration is abortive in the central nervous system following injury. Orchestrating microtubule dynamics has emerged as a promising approach to improve axonal regeneration. The microtubule severing enzyme spastin is essential for axonal development and regeneration through remodeling of microtubule arrangement. To date, however, little is known regarding the mechanisms underlying spastin action in neural regeneration after spinal cord injury. Here, we use glutathione transferase pulldown and immunoprecipitation assays to demonstrate that 14-3-3 interacts with spastin, both *in vivo* and *in vitro,* via spastin Ser233 phosphorylation. Moreover, we show that 14-3-3 protects spastin from degradation by inhibiting the ubiquitination pathway and upregulates the spastin-dependent severing ability. Furthermore, improving the interaction between 14-3-3 and spastin by Fusicoccin (FC-A) promotes neurite outgrowth and regeneration *in vitro*. Western blot and immunofluorescence results revealed that 14-3-3 protein is upregulated in the neuronal compartment after spinal cord injury *in vivo*. In addition, administration of FC-A not only promotes locomotor recovery, but also nerve regeneration following spinal cord injury in both contusion and lateral hemisection models. However, application of spastin inhibitor spastazoline successfully reverses these phenomena. Taken together, these results indicate that 14-3-3 is a molecular switch that regulates spastin protein levels, and 14-3-3/spastin pathway is an important target for regulation of microtubule dynamics for nerve regeneration after spinal cord injury.

Keywords: Spastin; Microtubule; Axon regeneration; 14-3-3; Spinal cord injury

Graphical Abstract

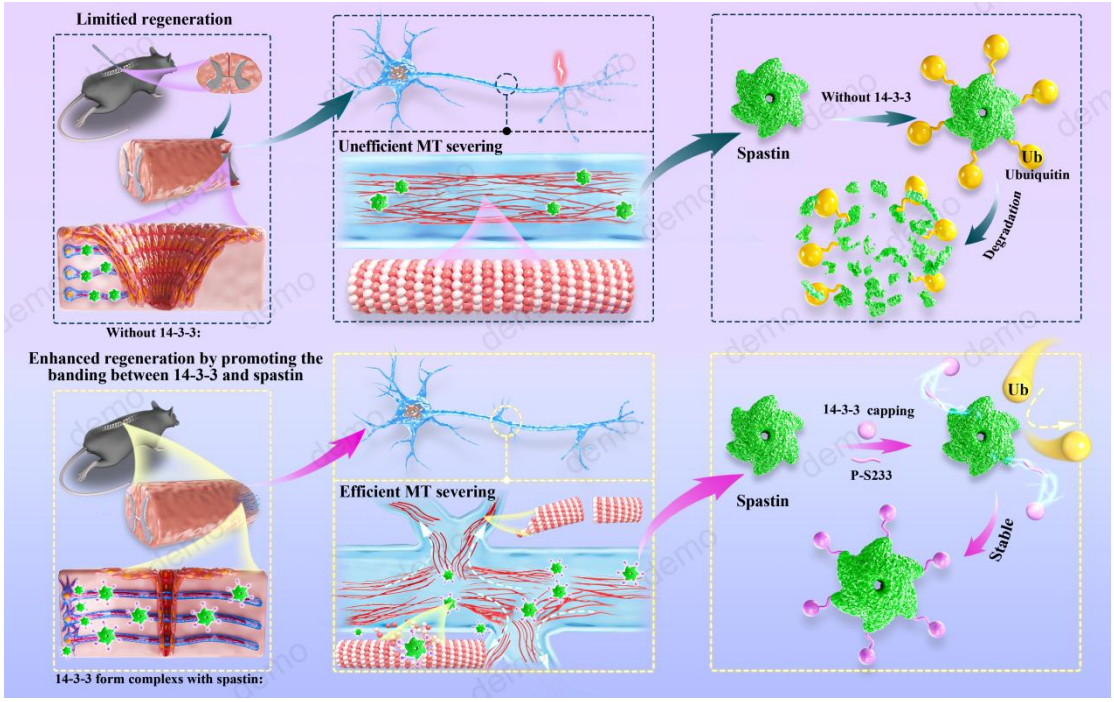

Introduction

Regeneration of the adult central nervous system neurons is difficult after injury, a phenomenon that results in permanent neurological impairments[1]. Researchers have attributed this not only to the highly inhibitory extrinsic environment at the injury site but also to limited cell-intrinsic growth capacity. Many studies have demonstrated that re-programming of growth-associated processes plays a key role in manipulation of axonal regeneration[2-4]. However, the specific mechanisms underlying axonal regeneration failure remain largely unknown. Cytoskeleton remodeling, including actin and microtubule (MT) reorganization, appears to be the key factors directing the fate of axonal regeneration and sprouting[5]. Notably, the retraction bulb of severed axons at the lesion site of the spinal cord needs a dynamic cytoskeleton for successful regeneration. Moreover, formation of axon collaterals from spared axons also needs dynamic cytoskeleton reorganization to form new neural circuits with the innervated neurons[6, 7]. Mechanistically, invasion by MTs can not only provide mechanical force, but also guide intracellular transport to regulate distribution of specific molecules, including mitochondria, peroxisomes, growth factors and other, and subsequently mediate axonal extension. Therefore, timely invasion of microtubules

can not only power the formation of a growth cone with competent growth ability from the retraction bulb, but also improve the process of axonal sprouting from the spared axons[8, 9]. Overall, manipulating MT dynamics is critical for boosting axon regeneration.

Spastin is encoded by SPG4 gene and its mutations were identified form the patients of hereditary spastic paraplegia (HSP)[10]. It is a MT severing enzyme (including spastin, katanin and fidgetin) which can cut long MTs into short fragments, a phenomenon that not only endows MTs with high dynamics but also mediates their subsequent turning and regrowth under physiological conditions[11]. Spastin has two major isoforms, namely M1 and M87, coded form different initial sites. Both isoforms are highly expressed in the spinal cord[12]. Moreover, spastin mutation lacking severing activity can lead to the degeneration of the corticospinal tracts in HSP patients. In addition, spastin is highly expressed in the central neuronal system (CNS) and essential for formation of axon branches as well as their extension during neural development[13, 14]. These evidences indicate that spastin plays an important role in axonal development and maintainence in the spinal cord. Intriguingly, several studies have demonstrated that spastin is necessary for successful axon regeneration, but not other severing enzyme like katanin and fidgetin[15]. Moreover, loss spastin function reportedly resulted in an almost complete failure of axon regeneration, suggesting that it plays a vital role in axon regeneration following spinal cord injury. Therefore, manipulating spastin expression may be an effective way to promote axon regeneration. However, efficient regeneration is dependent on the precise spastin dosage, with studies showing that excess spastin is toxic and may destroy the MT network, while low doses have been associated with insufficient MT severing which subsequently limits MT remodeling for regeneration[15, 16]. In this case, direct manipulation of the spastin gene may not be the most appropriate approach for promoting successful axon regeneration after the CNS injury. It is worth noting that posttranslational modifications, protein metabolism and protein-protein interactions are vital for regulating the protein's activity[17]. Therefore, elucidating the specific

molecular mechanism underlying spastin action is imperative to guiding future development of effective interventions to promote axon regeneration following damage to the CNS.

14-3-3 protein is a type of adaptor protein that play important roles in many signaling pathways through interaction with their substrates[18, 19]. For instance, it inhibits the ROS-induced cell death by interacting with FOXO transcription factors to prevent upregulation of many pro-apoptotic genes[20]. In mammals, seven isoforms, namely β、γ、ε、ζ、η、θ and σ, have been identified. They are not only highly preserved in the mammalian system, but also form a dimeric structure to interact with their substrates which are mostly phosphoproteins[21]. Previous studies have shown that spastin is phosphorylated in Ser233 which showed its potential for interaction with 14-3-3[22]. In addition, 14-3-3 protein is also highly expressed in CNS where it plays a vital role in both axonal growth and guidance. Previous studies have also demonstrated that 14-3-3 promotes cortical neurite outgrowth and axon regeneration[23, 24]. To date, however, the molecular mechanisms underlying its action in promotion of axon regeneration as well as its role in spinal cord injury remain largely unknown.

In this study, we demonstrate that 14-3-3 interacts with spastin to regulate its stability, thus controlling both neurite outgrowth and regeneration after injury. Our results reveal that 14-3-3 interacts with serine 233 in spastin, in a phosphorylation-dependent manner, thereby preventing its degradation by ubiquitination and upregulates the severing ability via spastin-mediated activity. Moreover, we found that enhancing this interaction via Fusicoccin (FC-A) application resulted in enhanced axon regeneration and locomotor improvement both in contusion model and in T10 lateral hemi-transection model of spinal cord injury. Collectively, our findings suggest 14-3-3/spastin pathway is a novel intervention target for axon regeneration after spinal cord injury.

Materials and methods

Animals

124 Sprague Dawley rats (P0) were used for primary hippocampal and cortical neuron
125 culture, whereas adult female mice (C57BL/6J, 6-8 weeks) were used to establish the
126 lateral hemi-transection model and the contusion model of spinal cord injury. Animals
127 were housed in a room, maintained at 22°C under a 12:12 h light/dark photoperiod,
128 and given food and water ad libitum. All animal treatments were carried out in strict
129 adherence to the guidelines by the National Institutes of Health's Guide for the Care
130 and Use of Laboratory Animals. The study protocol was approved by Jinan University
131 Institutional Animal Care and Use Committee. The number of animals utilized and
132 suffering were both reduced to the absolute minimum.

133 **Cell culture and transfection.** Dissociated hippocampi were digested with 2 mg/mL
134 papain and plated at a density of 1×10^4cells/cm^2 onto poly-D-lysine-coated coverslips
135 for primary hippocampal neuron culture. Cultures were kept alive in an incubator
136 humidified with 5% CO_2 at 37°C using Neurobasal-A media supplemented with 0.5
137 mM glutamine and 2% B27. Every three days, half of the cultural media was replaced.
138 Various plasmids were transfected with calcium phosphate at 2th day in vitro (DIV).
139 COS7 cells and human embryonic kidney (HEK) 293 cells were grown in a 5% CO_2
140 incubator at 37°C using Dulbecco's modified Eagle media with 10% fetal bovine
141 serum and 1% penicillin/streptomycin as supplemental ingredients. The constructs
142 were transfected into the COS7 cells and HEK293 cells using Lipofectemine 2000.
143 Cells were cultured for 24-36 hours after transfection before being harvested.

144 **Plasmids and constructs**

145 Several 14-3-3 isoforms were amplified in cDNA from Sprague Dawley rats via
146 Polymerase Chain Reaction (PCR) as previously described[14]. The amplicons were
147 inserted into the pCMV-Tag-2b or pGEX-5X-3 vector (Addgene). Spastin mutants
148 were generated using the Quickchange Kit (Agilent, Santa Clara, CA). R18 was
149 synthetized by IGE Biotechnology LTD（Guangzhou, China） and inserted into
150 pCDNA 3.1 vector. All constructs were verified by sequencing by IGE Biotechnology
151 LTD（Guangzhou, China）.

152 **Expression of recombinant proteins and GST-Pulldown assay**

153 Purification of GST fusion of 14-3-3 proteins and pulldown experiments were
154 performed as previously described[14, 25]. Briefly, GST-14-3-3s constructs
155 (Invitrogen) were transformed into *Escherichia coli* strain BL21 (DE3) strains.
156 Isopropy-D-thiogalactoside was incubated for 6 hours at 30°C to stimulate the
157 synthesis of fusion proteins. The bacteria were first centrifuged, then resuspended in a
158 mixture of protease inhibitors (Merck, Whitehouse Station, NJ). The cell suspension
159 was treated with 0.1% lysozyme, followed by 0.5% deoxycholic acid on ice for 20
160 min. The contents were, sonicated (10,000 rpm for 30 min), centrifuged and the
161 supernatant collected, then Glutathione-Sepharose beads (supplemented with 1%
162 Triton X-100) used to purify GST fusion proteins in the supernatant. Next, 5 μg of
163 GST-fusion protein was incubated with 400 μg of protein from the spinal cord (1 cm
164 around T10) of SD rats (P0) under gentle rotation, then centrifugated to collect the
165 GST-binding proteins. Western blot assay was then performed to quantify
166 GST-binding proteins.

167 **Immunoprecipitation and western blotting**.

168 Immunoprecipitation (IP) assays were carried out as previously described[26]. Briefly,
169 total cell extracts or tissues (1 cm around T10) were prepared by soaking them in 400
170 μL of lysis buffer for 30 minutes at 4 °C. The lysates were centrifuged at 10,000 rpm
171 for 10 minutes at 4 °C after a brief sonication. The extract was immunoprecipitated
172 with 2 μg antibodies against spastin, GFP, or Flag, and then incubated for 4 hours at
173 4 °C with 60 μL of protein G plus protein A/G agarose using continuous gentle
174 inversion. Three times, the immune complexes were pelleted and washed. Western
175 blot assay was performed to analyze the precipitated complexes. Western blot analysis
176 was carried out as previously described[14]. SDS-PAGE was used to separate the
177 lysates, which were then electrophoretically transferred to a polyvinylidene difluoride
178 membrane. Membranes were probed with primary antibodies at 4 °C overnight after
179 being blocked in Tris-buffered saline with 5% milk and 0.05% Tween. The
180 membranes were cleaned, incubated with goat anti-mouse or anti-rabbit secondary
181 antibodies that were horseradish peroxidase conjugated, and then visualized with

182 ECL-prime. Anti-spastin (1:1000, ABN368 from Millipore), anti-Pan 14-3-3 (1:1000,
183 #8312 from Cell Signaling Technology), anti-GFP (1:5000, Ab290 from Abcam),
184 anti-Flag (1:1000, F3165 from Sigma-Aldrich), anti-GAPDH (1:5000, AC002 from
185 ABclonal), and HRP conjugated goat-derived anti-rabbit or anti-mouse were the
186 antibodies used (1:5000, Abclonal).

187 **Scratch assay**

188 Rat cortical neurons were seeded in 96-well plates (30,000 cells per well), then a
189 plastic P10 pipet tip was used to scratch across the center of the well. Half the media
190 was aspirated out and replaced with fresh one every three days until the 7th DIV. The
191 wells were immediately filled with chemicals after scratching. The cultures were fixed
192 and stained with anti-βIII tubulin (1:1000, ab18207) the following day. Images of
193 axons stained with βIII tubulin were collected, imported in ImageJ, and the proportion
194 of neurites stained by βIII tubulin in the central 70% of the scratch were calculated.

195 **Lateral hemi-sectioning and contusion model of SCI**

196 The procedure for T10 lateral hemi-sectioning and contusion model was as
197 previously described[27, 28]. Briefly, mice were first anesthetized with 1.25%
198 2,2,2-tribromo ethanol (0.2 mL/100 g), via intraperitoneal injection for 3-4 min, then
199 a laminectomy performed near T10 after making a midline incision over the thoracic
200 vertebrae. The T10 level of the spinal cord was recognized by the anatomical
201 landmark which is parallel to the twelfth rib of the mice. For the hemi-sectioning
202 injury model, the right unilateral hemi-section was carefully performed using a scalpel
203 and microscissors, with care taken to avoid damaging the spinal cord dura. For the
204 contusion model, the nitrogen tank controlling the impactor tip was set at 18 psi or
205 124 kPa. A U-shaped stabilizer with the rat was loaded onto the stage of the Louisville
206 Injury System Apparatus (LISA) and the dura of the spinal cord was adjusted directly
207 under the impactor while monitored by the laser beam. Crash depth was adjusted to
208 1.0 mm for injury, and with time set to 0.5 s. Finally, the muscles were stitched and
209 the skin was stapled back together.

210 **Pharmacological interference with FC-A or spastin**

An equal volume of normal saline was intraperitoneally injected into SCI control mice. Mice were intraperitoneally injected with FC-A (Enzo life sciences, ALX-350-115) at a dose of 15 mg/kg starting immediately after SCI and every other day until end of the experiment. Mice were intraperitoneally injected with spastazoline (MedChemExpress, HY-111548) at a dose of 20 mg/kg, immediately after SCI then every other day until end of experiments.

Basso Mouse Scale

Two observers who were blind to the experimental groups conducted the Basso Mouse Scale (BMS) after the T10 SCI in accordance with a previously described procedure[29]. Mice were briefly left in an open field for 4 minutes to observe all visually perceptible signs of locomotor recovery. The scores were based on hind limb movements performed in an open field and included hind limb joint movement, weight support, plantar stepping, coordination, paw position, and trunk and tail control (0, full hind limb paralysis; 9, normal locomotion).

Catwalk analysis

According to previously described methods[30], the CatWalk XT 9.1 automated quantitative gait analysis system (Noldus Company, Netherlands) was also used to evaluate the locomotor recovery of mice after injury. Briefly, one week before surgery, mice were trained to walk in a single direction for the entire length of a darkened Catwalk chamber in a quiet room five times daily. Seven weeks after surgery, the mice were assessed five times using the same system. Gait regularity index and hindlimb contact area were recorded. The regularity index was calculated as the number of normal strides multiplied by four and then divided by the total number of strides; this value is ~100% in normal animals.

Footprint analysis

Footprint analysis was conducted before the mice were executed, using a previously described protocol[31]. Briefly, each animal's hindlimbs were first coated with nontoxic paint. The mice were then moved from a brightly illuminated starting box to a darkened one, by allowing them to walk through a narrow-custom-built

240 plexiglass trough (5 cm wide by 40 cm long), during which they left a trace of their
241 paw prints on the white sheet that overlaid the trough. The footprints were scanned,
242 and digitized images measured using Image J Pro Plus. Stride length was measured as
243 the distance between the adjacent hindlimbs, whereas stride width was taken as the
244 distance between the affected and the contralateral limbs. At least ten footprints per
245 side, from three sessions per animal, were measured for both parameters and their
246 average were calculated.

247 **Foot fault test**

248 The Parallel Rod apparatus was used in this test[32]. Summarily, mice were
249 positioned in the middle of the device, allowed to walk for three minutes during
250 which a video was captured. The test was performed by two observers who were
251 blinded to the experimental groups. One observer recorded the total number of steps
252 taken, while the other counted instances where each right hind limb slipped through
253 the rod. Three runs were recorded for every mouse.

254 **Motor evoked potential (MEP) recordings**

255 To assess SCI recovery, motor evoked potentials (MEPs) were recorded 7 weeks
256 after SCI according to previously described methods[30]. First, mice were
257 anesthetized with 1.25% 2,2,2-tribromo ethanol (0.2 mL/100 g). A craniotomy was
258 then performed to expose the M1 region of the motor cortex. Electrode penetration
259 was guided via a stereotaxic instrument to a depth of 700-1000 mm from the brain
260 surface to target corticospinal neurons in the sensorimotor cortex. The recording
261 electrode was placed on the gastrocnemius muscle and the reference electrode was
262 placed on the paraspinal muscle between the stimulation and recording points. A
263 ground electrode was attached to the tail. A single square-wave stimulus of 0.5 mA,
264 0.5 ms duration, 2 ms time delay, and 1 Hz was used. Amplitude was measured from
265 the beginning of the first response wave to its maximum point. All potentials were
266 amplified and acquired using a digital oscilloscope (Chengdu Instrument Factory,
267 Chengdu, China).

268 **Immunocytochemistry**

Cells were grown on coverslips and processed according to immunocytochemistry protocols as previously described[14]. Cells were fixed using freshly prepared 4% paraformaldehyde, followed by permeabilization with 0.1% Triton X-100 in TBS and blocking in 3% normal donkey serum. The cells on the coverslips were incubated with anti-GFP (1:1000, Ab290 form Abcam) or anti-α-tubulin(1:1000, ab7291 from Abcam) and then incubated with secondary antibody (Alexa Fluor 488 donkey anti-rabbit or Alexa Fluor 647 donkey conjugated to anti-goat immunoglobulin G (H+L) (Life Technologies). The coverslips were then mounted with DAPI (diamidino-2-phenylindole)-free Fluoro-Gel on glass slides (Electron Microscopy Sciences, USA). Cells were scanned using a 63x oil immersion objective mounted on a confocal microscope (LSM 710 Meta; Carl Zeiss). LSM 710 software was used to process the images after they were captured using sequential acquisition settings at a resolution of 1024 × 1024 pixels and a 12-bit depth.

Mice were administered consecutive transcardial infusions of 4% paraformaldehyde in PBS and 0.09% saline after being given a deep anesthetic. After tissue collection, post-fixation in 4% paraformaldehyde was applied overnight, and tissues were then immersed in 30% sucrose for two days to dehydrate them. Serial sagittal cryostat-sections were incubated at 4°C for at least 18 hours before being stained with primary antibodies in blocking buffer (3% goat serum and 5% donkey serum in 0.3% PBST). Alexa Fluor-coupled secondary antibodies (Life Technologies) diluted in blocking buffer were incubated for 2 hours at room temperature to perform the detection. Anti-GFAP (1:1000, GB11096 from Servicebio), anti-serotonin (1:5000, AB125 from Sigma-Aldrich), anti-neurofililament (1:200, A19084 from ABclonal) anti-Myelin Basic Protein (1:200, A11162 from ABclonal) anti-Brdu (1:200, A20790 from ABclonal), anti-Nestin (1:200, A11861 from ABclonal) and anti-NeuN (1:200, A19086 from ABclonal) were used. Images were scanned using a confocal microscope.

Statistical analysis

The analyses were carried out by Graphpad 8.4.0 software. Differences across

298 multiple groups were determined using One-way analysis of variance (ANOVA),
299 followed by Newman-Keuls post hoc tests for mean separations. $P \leqslant 0.05$ were
300 considered statistically significant.
301
302 **Results**
303 **14-3-3 protein interacts with spastin**
304 Spastin, a MTs severing enzyme, can cut long MTs into short fragments thereby
305 contributing to axonal elongation and branching. However, excess spastin levels by
306 gene manipulation can not only destroy the MT cytoskeleton but are also toxic to cells.
307 Unraveling the underlying mechanisms of spastin regulation under physiological
308 conditions may provide novel insights into the mode of axon regeneration following
309 CNS damage. In the present study, we performed GST-spastin pulldown assays on
310 lysates from the spinal cord tissue, then analyzed the binding complex via mass
311 spectrometry to determine the underlying molecular mechanisms of spastin. This
312 proteomics approach revealed14-3-3 as putative spastin-interacting proteins (Figure
313 1A & Figure S1A). Notably, 14-3-3 proteins consist of seven isoforms that are highly
314 conserved and act by targeting phosphoserine and phosphothreonine motifs of
315 substrate proteins. We have detected different many 14-3-3 peptides in the complex,
316 including LAEQAER, NLLSVAYK, and AVTEQGAELSNEER (Figure S1A).
317 Notably, these peptides were highly reserved among different isoforms (Figure S1B).
318 Next, we employed immunoprecipitation to determine the biochemical interaction
319 between 14-3-3 protein and spastin, and found that they endogenously interacted in
320 the spinal cord tissue (Figure 1B). To determine where the 14-3-3/spastin protein
321 complex functions in neurons, we double stained hippocampal neurons with spastin
322 and 14-3-3 antibody, and found that 14-3-3 was colocalized with spastin in the entire
323 cell compartment (Figure 1C), especially in the growth cone (Figure 1C1) and axon
324 shaft (Figure 1C2). Colocalization profiles are displayed in Figure 1D. To further
325 identify which isoform of 14-3-3 interacts with spastin, we generated six 14-3-3
326 isoforms in rats (β、γ、ε、ζ、η、θ), then purified GST fusion 14-3-3 proteins (Figure

327 1E). Results from a GST pull-down assay revealed that all 14-3-3 isoforms could
328 interact with spastin (Figure 1F). Subsequent co-immunoprecipitation assay results
329 confirmed that all 14-3-3 isoforms could form direct complexes with spastin (Figure
330 1G). Collectively, these results indicated that the 14-3-3 protein interacts with spastin
331 both *in vitro* and *in vivo*.

332 **14-3-3 binds to phosphorylated Ser 233 in spastin**

333 Next, we characterized the interaction region of spastin/14-3-3 binding. To this
334 end, we generated several GFP-tagged deletion constructs based on the modular
335 domain of spastin (Figure 2A), then co-expressed them with Flag-tagged 14-3-3 into
336 HEK293T cells. Co-immunoprecipitation assay, using GFP-Trap beads, revealed that
337 spastin fragments containing amino acids 85-316 but not those with 85-214
338 coprecipitated with 14-3-3 (Figure 2B). Next, we performed immunoprecipitation
339 assays using MTBD region (215-316 amino acids) of spastin with 14-3-3 and found
340 that 14-3-3 specifically binds to the MTBD region of spastin (Figure 2C).

341 Previous studies have shown that phosphorylation of the 14-3-3 substrate
342 regulates the binding of 14-3-3 proteins, although 14-3-3 can also bind to
343 non-phosphorylating proteins. To investigate whether spastin's phosphorylation state
344 affects its binding with 14-3-3, we performed pulldown assays by using GST-14-3-3
345 and GFP-spastin from transfected HEK293T cell extracts in the presence of broad
346 protein kinase staurosporine. Results revealed that presence of staurosporine markedly
347 weakened binding between spastin and 14-3-3, indicating that phosphorylation of
348 spastin is sufficient for the binding with 14-3-3 (Figure 2D). Next, we predicted five
349 putative 14-3-3 binding sites in spastin, namely amino acids 213-218, 230-235,
350 243-249, 425-460, and 559-564, which match the sequence motif of RSX(S/T)XP.
351 Combination with phosphorylation of spastin reported from previous MS data
352 (https://www.phosphosite.org/proteinAction.action?id=8325&showAllSites=true),
353 revealed two putative binding motifs (Ser233 and Ser562) in spastin as putative
354 targets for 14-3-3 binding (Figure 2E). Then, we mutated single Ser233 and Ser562 or
355 both to alanine in the spastin tagged with GFP and co-expressed them with

356 Flag-tagged 14-3-3 in HEK293T cells. Immunoprecipitation of the lysates, using an
357 antibody against GFP, revealed that spastin S562A can bind with 14-3-3, while spastin
358 S233A and spastin Pan A cannot (Figure 2F). Next, we transfected Ser233 mutation of
359 spastin (spastin S233A or spastin S233D) with flag tagged 14-3-3 and generated
360 Pearson's correlation coefficients. Results revealed that spastin S233D was markedly
361 colocalized with 14-3-3, with minimal colocalization with spastin S233A (Figure
362 2A-B). These results were consistent with those in Figure 3B-C, where Ser233 was
363 localized in the MTBD domain, further indicating that the binding of spastin-14-3-3
364 requires phosphorylation of spastin Ser233.

365 To examine whether Ser233 in spastin is involved in neurite outgrowth mediated
366 by spastin, wild type (GFP-spastin) or spastin Ser233 mutant （GFP-spastin S233A or
367 GFP-spastin S233D） was moderately expressed in primary hippocampal neurons at
368 2th DIV. Consistent with earlier results, spastin promoted neurite outgrowth, as
369 evidenced by both the length and total branches of neurite. A similar effect was
370 observed after transfection with spastin S233A. In contrast, we found a toxic effect
371 following transfection with spastin S233D (Figure 2G-I). Taken together, these data
372 suggests that the binding of 14-3-3 to the Ser233 in spastin has a direct influence on
373 the fate of neurite outgrowth.

374 **14-3-3 protects spastin from degradation via spastin S233 phosphorylation**

375 How does the interaction between 14-3-3 and Ser233 in spastin regulate neurite
376 outgrowth during neural development, and why does spastin S233D expression in
377 neurons cause toxic effect? Our earlier results demonstrated that spastin acts in a
378 dose-dependent manner, with excessive dosages found to destroy the microtubules
379 and generate a toxic effect. Here, we hypothesized that spastin S233D transfection
380 may upregulate expression of the spastin protein relative to WT and spastin S233A.
381 To further test whether 14-3-3 would affect spastin stability, we performed chase-time
382 assays via GFP-spastin overexpression, followed by treatment with Cycloheximide
383 (CHX) to inhibit protein synthesis. Results showed that expression of GFP-spastin
384 protein was markedly downregulated at 9 h after CHX treatment (Figure 3A). Next,

385 we co-expressed Flag-14-3-3 with GFP-spastin in the same treatment and found that
386 14-3-3 could significantly protect spastin from degradation after CHX treatment, even
387 after 24 h (Figure 3B-E). We also investigated whether 14-3-3 inhibited the
388 degradation in spastin S233 phosphorylation by transfecting with GFP-tagged spastin
389 S233A or S233D followed by CHX treatment. Results showed that 14-3-3 could
390 protect spastin (S233D), but not spastin (S233A), from degradation (Figure 3C-F).

391 A previous study demonstrated that spastin could be polyubiquitinated[33]. To
392 further determine whether 14-3-3 affected spastin's ubiquitination pathway, we
393 performed co-immunoprecipitation assays. GFP-spastin and Flag-ubiquitin were
394 transfected into HEK293T cells, co-expressed with 14-3-3 binding inhibitor R18 or
395 not . Results indicated that GFP-spastin could be ubiquitinated, while inhibiting the
396 binding of 14-3-3/spastin promoted spastin ubiquitination (Figure 5G). These results
397 indicated that 14-3-3 protects spastin from degradation by inhibiting the
398 ubiquitination pathway.

399 To evaluate whether spastin mediated microtubule severing activity, we
400 co-transfected GFP-spastin encoding plasmids into COS7 cells with or without
401 ubiquitin. COS7 cells are very flat, hence provide more spatial resolution compared to
402 neurons. Results showed that cells transfected with wild type spastin significantly
403 induced microtubule severing, as evidenced by almost no MT staining (Figure 3H),
404 while ubiquitin inhibited severing, leading to increased microtubule staining. Based
405 on these conditions, further transfection with 14-3-3 plasmid induced more
406 microtubule staining, indicating that 14-3-3 upregulates microtubule severing and the
407 process is mediated by spastin. Furthermore, we investigated whether this effect was
408 dependent on spastin S233 phosphorylation by replacing GFP-spastin with
409 GFP-spastin (S233A or S233D) during transfection. Results showed that 14-3-3 could
410 upregulate the severing ability of spastin S233D, but not S233A (Figure 3I), further
411 indicating that 14-3-3 binds to the phosphorylation of S233 in spastin and promotes
412 its microtubule severing ability. Collectively, these results suggest that 14-3-3 protein
413 protects spastin from degradation via spastin S233 phosphorylation.

414 **14-3-3/spastin complex regulates neurite outgrowth and regeneration after injury**

415 Next, we investigated how the interaction between 14-3-3 and spastin regulates
416 neurite outgrowth and regeneration by applying FC-A and R18 to either stabilize or
417 inhibit 14-3-3 binding. Previous studies have shown that FC-A and R18 interact with
418 14-3-3 protein by either stabilizing or inhibiting the binding of 14-3-3 with their
419 substrates by directly docking to the groove in the 14-3-3 proteins with highly
420 efficiency[34-36]. The structure of FC-A and R18 binding with 14-3-3 are shown in
421 Figure 4A. We also used another drug, spastazoline, to inhibit microtubule severing as
422 previously described[37, 38]. To test our hypothesis, we first explored whether FC-A
423 or R18 could enhance or inhibit the interaction between 14-3-3 and spastin by
424 co-immunoprecipitation with lysates of HEK293T cells, which had been transfected
425 with GFP-spastin and Flag-14-3-3 plasmids whether together with FC-A application
426 or R18 transfection. We found that FC-A could enhance the binding of 14-3-3/spastin,
427 as evidenced by more intense bands compared to no FC-A application, whereas R18
428 could efficiently inhibit the binding of 14-3-3/spastin with almost no binding was
429 detected (Figure 4B). Subsequently, we used FC-A together with spastazoline to
430 examine the effects of 14-3-3/spastin protein complex on neurite outgrowth and
431 regeneration.

432 Since 14-3-3 proteins play important roles in inhibition of ROS-induced cell
433 death, we first explored the effect of 14-3-3/spastin binding in neurite outgrowth and
434 repair under glutamate circumstances. Briefly, we established a neural injury model as
435 previously described[39], and found that they had numerous swellings and breakages
436 on the neurite, indicative of successful establishment of an injury model (Figure 4C).
437 After injury, FC-A was administered into primary hippocampal neurons during the
438 developmental stage 2, combination with application of spastin inhibitor spastazoline
439 which had been confirmed by previous study[37]. Results demonstrated that FC-A
440 could promote neurite outgrowth, both with regards to lengths and branches, after
441 glutamate-induced injury, while this promoting effect was abolished following
442 spastazoline administration (Figure 4D-G). A similar effect was observed in neurons

443 without glutamate induced injury (Figure S4). In contrast, transfection of R18 resulted
444 in an inhibitory effect on neurite outgrowth, but this was rescued with moderate
445 spastin expression after injury (Figure 4D-J). A similar trend was observed in neurons
446 without glutamate-induced injury (Figure S5). Collectively, these results suggest that
447 14-3-3 protein promotes the repair of injured neuron through the interaction with
448 spastin.

449 Next, we investigated the effect of enhanced 14-3-3/spastin binding on neurite
450 regeneration. Briefly, cortical neurons were grown at the 7th DIV then subjected to
451 scratch assays by drawing a line over the coverslips using a pipet tip. Neurons were
452 then treated with either FC-A or spastazoline for 36 hours. Results showed that FC-A
453 markedly improved neurite regeneration consistent with previous study[34], while
454 spastazoline application almost abolished the enhanced effects of regeneration (Figure
455 4K-L). To further quantify the extend of axon regeneration across each group, we
456 treated cortical neurons with either FC-A or spastazoline for 24 hours, then quantified
457 the longest regenerative axons. Results revealed similar effects (Figure S6). Taken
458 together, these results indicate that spastin-dependent severing is a prerequisite for the
459 enhancement of neurite regeneration mediated by FC-A.

460 **FC-A-mediated nerve regeneration after SCI requires spastin activation by**
461 **targeting MTs**

462 Given that 14-3-3 plays vital roles in neurite outgrowth and axonal
463 regeneration[40], we then hypothesized that 14-3-3 could be involved in the recovery
464 of spinal cord injury. To test this hypothesis, we established a spinal contusion injury
465 model and then employed western blot assay to quantify levels of 14-3-3 protein
466 following spinal cord injury. Results revealed that 14-3-3 was upregulated at 3th and
467 7th days post injury (DPI), but downregulated at 14 DPI. The 14-3-3 protein level
468 then reached a peak level at 30 DPI (Figure 5A-B). Moreover, immunostaining results
469 indicated that 14-3-3 protein upregulation was principally colocalized in the neuronal
470 compartment (βIII-tubulin labeled) (Figure 5C). Previous studies have demonstrated
471 that neurons were surrounded by inhibitory microenvironment 2 weeks after spinal

472 cord injury, our results also showed a slightly decrease at 14 DPI, indicating that
473 14-3-3 acts as an intrinsic switch for neural repair. Moreover, 14-3-3 was reported to
474 be upregulated and acted as a biomarker for diagnosis of Creutzfeldt-Jakob
475 disease[41]. Our results revealed that levels of 14-3-3 protein remained high even at
476 30 DPI, indicating that 14-3-3 plays an important role in the recovery of spinal cord
477 injury.

478 Enhancing the 14-3-3/spastin interaction mediated by FC-A can promote neurite
479 outgrowth and regeneration suggesting that it can be used to promote neurite regrowth
480 after injury *in vivo*. We therefore attempted to investigate whether FC-A could
481 improve nerve regrowth after spinal cord injury in a contusion injury model. FC-A
482 was administrated via intraperitoneal injection following SCI in mice. As shown in
483 figure 5D, H&E and LFB (Luxol fast blue stain) staining showed that the lesion site in
484 the injury group presented the destroyed tissue structure with loss of myelination.
485 Intriguingly, we found the tissue structure appeared to be normal and the area of
486 demyelination in the lesion site strongly decreased in the FC-A group. In addition, in
487 the spastazoline group, the lesion site appeared to be discontiguous, and application of
488 spastazoline reversed the protective effect on spinal cord demyelination. Next, we
489 further investigated nerve regeneration by immunostaining with NF (Neurofilament)
490 and 5-HT, which were co-stained with GFAP (astrocyte marker). As shown in figure
491 5E, the border of the spinal cord lesion site was marked with astrogliosis ($GFAP^{+}$),
492 and the neurofilament and 5-HT immunogenicity in the lesion site were almost
493 abolished compared to the uninjured area, indicating that the spinal cord contusion
494 injury model was successfully established. Interestingly, in the FC-A group, we
495 observed that the astrogliosis in the lesion site was attenuated and we found a great
496 deal of neurofilaments and 5-HT signals passing through the lesion site (Figure 5E,
497 boxed in E2), indicating that the application of FC-A enhanced the nerve regeneration
498 after injury. In the spastazoline group, we also observed tissue discontinuity, which is
499 consistent with figure 5D, and almost no NF and 5-HT were found across the lesion
500 site. Moreover, the application of spastazoline abolished the FC-A mediated nerve

501 regeneration after SCI. These results suggest that FC-A-mediated axonal regeneration
502 after SCI requires the activation of spastin function.

503 In order to further confirm whether the intervention of 14-3-3/spastin pathway by
504 FC-A and spastazoline mediates nerve regeneration after spinal cord injury by
505 targeting MTs at the site of spinal cord injury, acetylated tubulin and β-tubulin were
506 stained to label stale MTs (Lacking of dynamics) and total MTs. As shown in figure
507 S7 A, the intensity of acetylated microtubules was remarkable decreased in the lesion
508 site. Moreover, there was a clear boundary of acetylated MTs between the lesion site
509 and the uninjured area. This may be ascribed to the activation of cell proliferation in
510 the injured area after spinal cord injury which needs dynamic microtubules.
511 Interestingly, we found the boundary of acetylated microtubules near the damaged
512 area was unclear after application of FC-A, and the intensity of acetylated
513 microtubules significantly decreased compared with the injury group, indicating that
514 microtubules tended to be a dynamic state. However, after the application of
515 spastazoline, the proportion of acetylated microtubules in the injury site increased
516 significantly, and the boundary of acetylated microtubules in the injured area was
517 unclear, indicating that the application of spastazoline led to a significant increase in
518 the stability of the microtubules. In addition, the application of spastazoline can
519 significantly reverse the enhancement of microtubule dynamics mediated by FC-A
520 (Figure 5F). These experiments indicated that the administration of FC-A mediate
521 nerve regeneration after spinal cord injury through the 14-3-3/spastin pathway by
522 affecting the MTs dynamics. In addition, these evidences also indicated indirectly that
523 the FC-A and spastazoline can pass through the blood-brain barrier to reach the site of
524 spinal cord injury.

525 **FC-A-mediated locomotor function improvement after SCI requires spastin**
526 **participation**

527 Since FC-A promotes nerve regeneration after spinal cord injury by affecting the
528 14-3-3/spastin pathway, we then investigated whether it could mediate the recovery of
529 locomotor function after SCI. Therefore, we performed several experiments to verify

530 whether the application of FC-A could affect the locomotor function recovery after
531 SCI (Fig. 6A). Catwalk analysis showed that the maximum contact area of the mice in
532 the FC-A group was significantly larger than that in the injury group, and this
533 phenomenon was reversed after the application of spastazoline (Figure 6B&E). The
534 regularity index (Calculated as the number of normal strides multiplied by four and
535 then divided by the total number of strides; this value is ~100% in normal animals)
536 also had a similar phenomenon. The gait of the hindlimbs of mice in the FC-A group
537 was more coordinated than that of the mice in the injury group (Fig. 6C), and the
538 regularity index was statistically enhanced compared with the injury group (Fig. 6G).
539 This phenomenon was also significantly suppressed after the application of
540 spastazoline. We further evaluated the motor function after spinal cord injury by BMS
541 score (Fig. 6D). We found that the BMS scores of the mice in the FC-A group was
542 significantly improved compared with the mice in the injury group, and peaking after
543 35 days, while spastazoline reversed the improvement of locomotor function. At the
544 same time, we used the footprint test to analyze the motor function of the mice (Fig.
545 6F). The experimental data showed that the paw trailing phenomenon of the
546 hindlimbs in the FC-A group was significantly improved compared with the injury
547 group, and the stride length was significantly increased. This improvement was also
548 significantly suppressed by application of spastazoline (Fig. 6H). Finally, we
549 attempted to verify whether the spinal neural circuits in mice were remodeled by
550 examining the motor-evoked potentials (Stimulation at the sensorimotor cortex in the
551 M1 region and receive signals at the site of gastrocnemius). Our experimental results
552 showed that the MEP current amplitude decreased significantly after spinal cord
553 injury, while the current amplitude in the FC-A group significantly increased
554 compared with the injury group. And the improvement effect was significantly
555 weakened after the application of spastazoline, indicating that FC-A mediates the
556 remodeling of neural circuits after spinal cord injury by affecting the 14-3-3/spastin
557 pathway.

558 **Enhancing the 14-3-3/spastin pathway by FC-A stimulates the repair of SCI in a**

559 **T10 lateral hemisection model**

560 We have clarified the important role of 14-3-3/spastin pathway in the repair of
561 spinal cord injury in the contusion model. In order to further observe the axon
562 regeneration after spinal cord injury, we performed a spinal right lateral hemisection
563 at the T10 level to eliminate the right side of axonal projections. Neurotransmission of
564 serotonin (5-HT) in the spinal cord is required for the modulation of sensory, motor,
565 and autonomic functions and can influence the response to spinal cord injury[42, 43].
566 In addition, studies have reported that the 5-HT fibers have strong regenerative
567 capacity and involved in the regulation of neuronal activity[43]. Thus, we explored
568 the 5-HT immunoactivity in spinal cord tissues isolated on 17 DPI. In the control SCI
569 group, 5-HT-positive axons were significantly upregulated in the injury site, and to
570 some extent in the rostral site. Interestingly, we found much stronger 5-HT staining in
571 the lesion site of FC-A group and rostral site of injury compared with the SCI control
572 group, indicating that the FC-A promoted the regeneration of 5-HT positive axons *in*
573 *vivo*. However, few 5-HT signals were found in the lesion site, also in the rostral site
574 in the spastazoline group. In addition, the FC-A promoting effects of 5-HT axonal
575 regeneration were significantly weakened by the combined application of spastazoline
576 (Figure 7A&C).

577 We further investigated the immunoactivity of neurofilament and myelin basic
578 protein (MBP) in the white matter of the lesion site to evaluate axonal regeneration
579 and the extend of remyelination. Neurofilament are cytoskeletal proteins that are
580 expressed abundantly in the cytoplasm of axonal fibers in the CNS[44]. The MBP
581 forms and maintains the structure of the compact myelin sheath which then regulates
582 axonal function[45]. Our results revealed that FC-A could enhance the regeneration of
583 neurofilaments which were largely colocalized with MBP, whereas spastazoline
584 alleviated this effect (Figure 7B&D). Collectively, these results suggest that FC-A
585 promotes axonal regeneration which is dependent on activation of spastin microtubule
586 severing.

587 Previous studies have reported that the proliferation of neural stem/progenitor

588 cells is also reactivated and contributes to synapse formation following spinal cord
589 injury[46, 47]. Since spastin is a microtubule severing enzyme involved in cell
590 division. Thus, we explored the possibility that whether 14-3-3/spastin complex
591 participates in proliferation process of neural stem/progenitor cells. Therefore, spinal
592 cord tissues from the lesion site were stained with Nestin, Brdu and NeuN.
593 Intriguingly, we found that FC-A treatment after SCI significantly increased the
594 expression of Nestin (Figure S9A-B) and Brdu (Figure S10), and these effects were
595 abolished by spastazoline treatment. These results demonstrated that the
596 14-3-3/spastin complex contributed to the proliferation of neural stem/progenitor cells
597 thereby improving recovery after spinal cord injury.

598 We also further examined whether FC-A administration altered the motor
599 function after SCI in this lateral hemisection injury model. Mice with SCI in all
600 groups exhibited paralysis in the right hindlimb after hemisecion which confirmed the
601 successful establishment of the lateral hemisection SCI model. For mice in SCI
602 control group, the BMS scores gradually improved to ~4 by 16 DPI. In contrast, the
603 scores of mice in the FC-A group indicated an improvement in locomotor function
604 which was impaired in the spastazoline group. Moreover, the improvement in
605 locomotor function following administration of FC-A diminished when spastazoline
606 was administered (Figure 7E). We further analyzed the footprint of mice with SCI and
607 calculated the length or width of strides (Figure S11). We found that stride length
608 improved in mice of the FC-A group but it was reduced in the spastazoline group
609 although not significantly. The improvement induced by FC-A diminished when
610 co-treated with spastazoline (Figure 7G). Notably, there was no significant difference
611 in stride width between the groups (Figure 7H). Similar effects were observed in the
612 foot fault scan experiment. The faults of right hindlimb significantly decreased in the
613 FC-A group and increased in the spastazoline group (Figure 7F). The improvement of
614 hindlimb fault in mice administered with FC-A diminished following the application
615 of spastazoline. The representative movements of mice in each group were recorded
616 in Movie S1 (Control group), Movie S2 (Injury group), Movie S3 (FC-A group),

617 Movie S4 (Spastazoline group) and Movie S5 (FC-A+Spastazoline group). We also
618 explored whether the stability of MTs was altered by administration of FC-A and
619 spastazoline in the spinal cord injury model. We found that the ratio of acetylated
620 tubulin to total tubulin was significantly increased in the SCI group, decreased in the
621 FC-A group, and upregulated in the spastazoline group, which further confirmed the
622 successful delivery of drugs to the lesion site (Figure S8). These findings suggested
623 that FC-A was effectively delivered to the spinal cord tissue and improved the
624 locomotor function of mice with SCI, through 14-3-3/spastin pathway activation
625 mechanism.
626

627 **Discussion**

628 The limited cell intrinsic regrowth capability at the injury site of CNS damage or
629 disease results in failure of axonal regeneration. Recent studies have demonstrated
630 that the remodeling of microtubule dynamics was necessary for promoting axon
631 regeneration[48, 49]. Spastin is a microtubule (MT) severing enzyme which cuts long
632 MTs into short fragments for local MTs remodeling and thus could be administrated to
633 promote axon regeneration[50]. In this study, we aimed to reveal the regulatory
634 molecular mechanisms of spastin and its role in the recovery of spinal cord injury. We
635 found that 14-3-3 interacted with spastin by targeting the phosphorylation of Ser233,
636 protecting spastin against ubiquitin-mediated degradation, thus up-regulated the
637 spastin-dependent microtubule severing activity. Moreover, enhancing the
638 14-3-3/spastin interaction by FC-A promoted the neurite outgrowth and regeneration.
639 In adult mice with of SCI (both in contusion and lateral hemisection spinal cord injury
640 model), we found that enhanced 14-3-3/spastin binding promoted the recovery of
641 locomotor function and axonal regeneration. Therefore, we postulated that the
642 14-3-3/spastin pathway is an attractive target for improving axonal regeneration and
643 locomotor recovery after SCI.

644 To date, the severing activity induced by spastin has been well characterized[51,
645 52] and reported to be essential in the formation of axon branches and axonal

646 extension[53, 54]. Studies have also shown that spastin regulates axon regeneration in
647 a dose dependent manner. Of note, during regeneration, the cytoskeleton undergoes
648 remodeling, suggesting that manipulation of MTs dynamics by spastin may be a
649 potential approach for controlling neural regeneration. However, efficient
650 regeneration is dependent on the precise spastin dosage. Therefore, understanding the
651 underlying regulatory mechanism of spastin is pivotal for identifying therapeutic
652 targets in CNS. In this study, LC-MS based proteomics analysis was performed and
653 proteins that bind spastin were screened to investigate the regulatory mechanisms of
654 spastin during CNS damage (Figure 1A&S1). Among the identified binding proteins,
655 14-3-3 proteins had high scores and was found to interact with spastin in the spinal
656 cord (Figure 1B). This revealed the binding of 14-3-3 proteins to spastin in the injured
657 spinal cord. Of note, MS data from a previous study also showed that the spastin
658 peptides were present in the binding peptides with 14-3-3 agonist Fusicoccin[50],
659 which confirmed the important relevance between these two proteins. Considered that
660 both 14-3-3 and spastin were found to regulate axon outgrowth and regeneration,
661 colocalization analysis were performed. The results indicated that 14-3-3 interacted
662 with spastin to affect axon development. In addition, GST pulldown and
663 co-immunoprecipitation assays further verified the interaction between all 14-3-3
664 isoforms and spastin (Figure 1F-H). Also, the binding between 14-3-3 and spastin was
665 further characterized which showed that Ser233 in spastin was responsible for the
666 binding, and could directly influence the fate of neurite outgrowth (Figure 2).
667 Previously, it was found that spastin was phosphorylated at Ser233 (human Ser268)
668 by HIPK2 and this process was vital for successful abscission and the loss of HIPK2
669 exhibited a protective effect on neurons[55]. Our western blotting results showed that
670 HIPK2 was expressed at 9th DIV in the brain tissue (not presented), suggesting that
671 there may be other kinases that regulate Ser233 phosphorylation during neural
672 development. Therefore, we have well established the model of the 14-3-3/spastin
673 binding which could be the intervention target for regulating the MT severing
674 mediated by spastin.

675 The regulatory mechanisms that control the MT severing activity mediated by
676 spastin are largely unknown. In our previous study, spastin protein expression levels
677 and its severing effect were regulated at post-transcriptional levels, such as
678 micoRNA-30[53] and SUMOylation[14]. In this study, we found that 14-3-3
679 interacted with spastin from the perspective of protein-protein interactions, and we
680 showed that 14-3-3 prevented the ubiquitin-mediated degradation of spastin by
681 inhibiting the ubuiquitin pathway and phosphorylation of Ser233 was crucial to this
682 process. Our results showed that Ser233 de-phosphorylation lowered the protein
683 stability, consistent with findings from a recent study[33], and our study further
684 illustrated the molecular mechanisms of this phenomenon. In addition, we observed
685 that 14-3-3 up-regulated the microtubule severing activity of spastin through
686 interacting with its phosphorylation at Ser233. Based on this mechanism, we proposed
687 a model in which Ser233 is phosphorylated during the binding of 14-3-3 to spastin,
688 thereby disrupting the spastin/ubiquitin binding, ultimately affecting the stability of
689 spastin and subsequent neurite outgrowth and regeneration. Similar mechanisms were
690 reported for doublecortin[56], cdt2[57], p21[58] and other proteins[59]. For example,
691 14-3-3ε was found to interact with threonine 42 in doublecortin which protected it
692 from degradation by inhibiting its ubiquitination. In this way, it regulated the
693 doublecortin-regulated microtubule stability and neurite initiation process[57]. In this
694 part, we validated that 14-3-3 stabilized the protein levels of spastin and enhanced the
695 MT severing activity mediated by spastin which was similar to the mechanism of
696 14-3-3/cdt2 binding.

697 Since 14-3-3 proteins are adaptor proteins that are highly expressed in neural
698 tissues, they are important regulators of neural development[60, 61]. Using a
699 well-established 14-3-3/spastin interaction model, we found that promoting the MT
700 dynamics by enhancing the interaction of 14-3-3/spastin could enhance neurite
701 outgrowth and regeneration. This accelerated neurite outgrowth and repair following
702 FC-A application by facilitating the binding of 14-3-3/spastin (Figure 4). In
703 accordance with previous findings, 14-3-3 proteins can promote neurite outgrowth

704 and axonal regeneration[34]. In our study, we further demonstrated that enhanced
705 14-3-3/spastin interaction by FC-A favored neurite outgrowth and regeneration, but
706 this effect was blunted by spastazoline treatment. Spastazoline was designed to
707 compete with the AAA domain of spastin and this effectively abolished the severing
708 activity mediated by spastin[37]. The results also demonstrated that the normal
709 severing activity mediated by spastin was required for neurite outgrowth and
710 regeneration (Figure 4). These findings open a new window for developing
711 spastin-based agents for accelerating axon regeneration after injury.

712 So far, few studies have investigated the relationship between spastin and neural
713 regeneration in CNS diseases, such as spinal cord injury or brain injury. However,
714 many studies have elucidated its indispensable role in the process of axon
715 regeneration[50]. Our study first indicate that functional spastin is required for axon
716 regeneration and locomotor recovery after spinal cord injury (Figure 5&6). Moreover,
717 14-3-3 was upregulated at 3 and 7 DPI, and was even higher at 30 DPI in the neuronal
718 compartment, suggesting that 14-3-3 has an important role in neural repair after spinal
719 cord injury (Figure 5). Using the model of 14-3-3/spastin interaction, we further
720 elucidated the mechanism by which FC-A administration regulates the recovery of
721 spinal cord injury by targeting MTs. Fusicoccin-A (FC-A) is a fusicoccane, a small
722 molecule produced by the *Phomopsis amygdali fungus* that stabilizes the binding of
723 14-3-3 to its substrates[62]. The crystal structure of FC-A bound to 14-3-3 has already
724 revealed the efficiency of the enhancement of FC-A in the interaction between 14-3-3
725 and their substrate[63]. In addition, FC-A has been reported to promote axonal
726 regeneration in mammals[34], although the mechanisms are rarely elusive. In this
727 study, we found that FC-A enhanced the 14-3-3/spastin interaction and FC-A
728 administration restored nerve regeneration and locomotor recovery after SCI (in both
729 contusion and lateral hemisection spinal cord injury model), but these improvements
730 were abolished following spastazoline administration (inhibiting the MT severing by
731 direct competing with AAA domain of spastin[37]), suggesting the important role of
732 14-3-3/pathway in the neural circuts remolding after SCI. This phenomenon was

733 further confirmed by examined the ratio of acetylated tubulin in the lesion site of SCI,
734 and our results showed the intervention of 14-3-3/spastin pathway by FC-A and
735 spastazoline could significantly affect the MTs dynamics in the lesion site which
736 indirectly demonstrated the efficient delivery of these drugs to the spinal cord across
737 the blood brain barrier. Since spastin plays an essential role in cell abscission, and the
738 activation of 14-3-3/spastin pathway by FC-A promoted the proliferation of neural
739 stem/progenitor cells (Figure S8&S9) thereby support axonal regeneration. These
740 results also support that promoting 14-3-3/spastin interaction by FC-A enhanced
741 axonal regeneration after spinal cord injury, and the microtubule severing independent
742 of spastin was important in this process. Therefore, our findings present
743 14-3-3/spastin pathway as a novel intervention for accelerating nerve regeneration
744 after spinal cord injury.

745 In summary, we proposed the 14-3-3/spastin binding model for manipulating
746 microtubule dynamics and can be an effective intervention for promoting recovery of
747 spinal cord injury. In addition, our results indicate that 14-3-3 and spastin are
748 important regulators for nerve regeneration and modulating the interaction between
749 14-3-3 and spastin may be an effective strategy for the treatment of spinal cord injury.

750

751

752 **Abbreviations**

753 5-HT, 5-hydroxytryptamine; Cdt2, cell division cycle protein; CNS, central neuronal
754 system; DPI, days post injury; ECL, enhanced chemiluminescence; FOXO, forkhead
755 box transcription factors; GFAP, glial fibrillary acidic protein; GFP, green fluorescent
756 protein; HIPK2, homeodomain interacting protein kinase 2; HSP, hereditary spastic
757 paraplegia; IP, Immunoprecipitation; MBP, Myelin basic protein; MS, mass
758 spectrometry; MT, microtubule; ROS, reactive oxygen species;

759

760 **Acknowledgement**

761 This work was supported by the Natural Science Foundation of China (grant nos.

82102314, 31900691, and 32170977), the Natural Science Foundation of Guangdong Province (grant nos. 2022A1515010438 and 2022A1515012306), Science and Technology Projects in Guangzhou (grant nos. 202201020018) and Project funded by China Postdoctoral Science Foundation (2023M731320).

Competing interests

The authors declare no conflict of interest.

Data availability

The datasets obtained and/or analysed in the current study are available from the corresponding author upon reasonable request.

Reference

1. Curcio M, Bradke F. Axon Regeneration in the Central Nervous System: Facing the Challenges from the Inside. Annual review of cell and developmental biology. 2018; 34: 495-521.

2. Hilton BJ, Husch A, Schaffran B, Lin TC, Burnside ER, Dupraz S, et al. An active vesicle priming machinery suppresses axon regeneration upon adult CNS injury. Neuron. 2022; 110: 51-69.e7.

3. Mahar M, Cavalli V. Intrinsic mechanisms of neuronal axon regeneration. Nature reviews Neuroscience. 2018; 19: 323-37.

4. Clark CEJ, Liu Y, Cooper HM. The Yin and Yang of Wnt/Ryk axon guidance in development and regeneration. Science China Life Sciences. 2014; 57: 366-71.

5. Jin Y. Unraveling the mechanisms of synapse formation and axon regeneration: the awesome power of C. elegans genetics. Science China Life Sciences. 2015; 58: 1084-8.

6. Pinto-Costa R, Sousa SC, Leite SC, Nogueira-Rodrigues J, Ferreira da Silva T, Machado D, et al. Profilin 1 delivery tunes cytoskeletal dynamics toward CNS axon regeneration. The Journal of clinical investigation. 2020; 130: 2024-40.

7. Crunkhorn S. CNS injury: Microtubule stabilizer repairs spinal cord injury. Nature reviews Drug discovery. 2015; 14: 310.

8. Chen L, Rolls MM. Microtubule deacetylation sets the stage for successful axon regeneration. The

791 EMBO journal. 2012; 31: 3033-5.
792 9. Vargas EJM, Matamoros AJ, Qiu J, Jan CH, Wang Q, Gorczyca D, et al. The microtubule
793 regulator ringer functions downstream from the RNA repair/splicing pathway to promote axon
794 regeneration. Genes & development. 2020; 34: 194-208.
795 10. Shribman S, Reid E, Crosby AH, Houlden H, Warner TT. Hereditary spastic paraplegia: from
796 diagnosis to emerging therapeutic approaches. The Lancet Neurology. 2019; 18: 1136-46.
797 11. Liu Q, Zhang G, Ji Z, Lin H. Molecular and cellular mechanisms of spastin in neural development
798 and disease (Review). International journal of molecular medicine. 2021; 48.
799 12. Salinas S, Carazo-Salas RE, Proukakis C, Schiavo G, Warner TT. Spastin and microtubules:
800 Functions in health and disease. J Neurosci Res. 2007; 85: 2778-82.
801 13. Lopes AT, Hausrat TJ, Heisler FF, Gromova KV, Lombino FL, Fischer T, et al. Spastin depletion
802 increases tubulin polyglutamylation and impairs kinesin-mediated neuronal transport, leading to
803 working and associative memory deficits. PLoS biology. 2020; 18: e3000820.
804 14. Ji ZS, Liu QL, Zhang JF, Yang YH, Li J, Zhang GW, et al. SUMOylation of spastin promotes the
805 internalization of GluA1 and regulates dendritic spine morphology by targeting microtubule dynamics.
806 Neurobiology of disease. 2020; 146: 105133.
807 15. Stone MC, Rao K, Gheres KW, Kim S, Tao J, La Rochelle C, et al. Normal spastin gene dosage is
808 specifically required for axon regeneration. Cell reports. 2012; 2: 1340-50.
809 16. Rao K, Stone MC, Weiner AT, Gheres KW, Zhou C, Deitcher DL, et al. Spastin, atlastin, and ER
810 relocalization are involved in axon but not dendrite regeneration. Molecular biology of the cell. 2016;
811 27: 3245-56.
812 17. Martins-Marques T, Ribeiro-Rodrigues T, Batista-Almeida D, Aasen T, Kwak BR, Girao H.
813 Biological Functions of Connexin43 Beyond Intercellular Communication. Trends in cell biology. 2019;
814 29: 835-47.
815 18. Fu W, Hu W, Yi YS, Hettinghouse A, Sun G, Bi Y, et al. TNFR2/14-3-3ε signaling complex
816 instructs macrophage plasticity in inflammation and autoimmunity. The Journal of clinical investigation.
817 2021; 131.
818 19. Fu W, Hettinghouse A, Chen Y, Hu W, Ding X, Chen M, et al. 14-3-3 epsilon is an intracellular
819 component of TNFR2 receptor complex and its activation protects against osteoarthritis. Annals of the

820 rheumatic diseases. 2021; 80: 1615-27.
821 20. Nielsen MD, Luo X, Biteau B, Syverson K, Jasper H. 14-3-3 Epsilon antagonizes FoxO to control
822 growth, apoptosis and longevity in Drosophila. Aging cell. 2008; 7: 688-99.
823 21. Park E, Rawson S, Li K, Kim BW, Ficarro SB, Pino GG, et al. Architecture of autoinhibited and
824 active BRAF-MEK1-14-3-3 complexes. Nature. 2019; 575: 545-50.
825 22. Pisciottani A, Biancolillo L, Ferrara M, Valente D, Sardina F, Monteonofrio L, et al. HIPK2
826 Phosphorylates the Microtubule-Severing Enzyme Spastin at S268 for Abscission. Cells. 2019; 8.
827 23. Kaplan A, Morquette B, Kroner A, Leong S, Madwar C, Sanz R, et al. Small-Molecule
828 Stabilization of 14-3-3 Protein-Protein Interactions Stimulates Axon Regeneration. Neuron. 2017; 93:
829 1082-93 e5.
830 24. Yam PT, Kent CB, Morin S, Farmer WT, Alchini R, Lepelletier L, et al. 14-3-3 proteins regulate a
831 cell-intrinsic switch from sonic hedgehog-mediated commissural axon attraction to repulsion after
832 midline crossing. Neuron. 2012; 76: 735-49.
833 25. Ji Z, Zhang G, Chen L, Li J, Yang Y, Cha C, et al. Spastin Interacts with CRMP5 to Promote
834 Neurite Outgrowth by Controlling the Microtubule Dynamics. Developmental neurobiology. 2018; 78:
835 1191-205.
836 26. Ji ZS, Li JP, Fu CH, Luo JX, Yang H, Zhang GW, et al. Spastin interacts with collapsin response
837 mediator protein 3 to regulate neurite growth and branching. Neural regeneration research. 2021; 16:
838 2549-56.
839 27. Patel M, Li Y, Anderson J, Castro-Pedrido S, Skinner R, Lei S, et al. Gsx1 promotes locomotor
840 functional recovery after spinal cord injury. Molecular therapy : the journal of the American Society of
841 Gene Therapy. 2021; 29: 2469-82.
842 28. Liu Y, Wang X, Li W, Zhang Q, Li Y, Zhang Z, et al. A Sensitized IGF1 Treatment Restores
843 Corticospinal Axon-Dependent Functions. Neuron. 2017; 95: 817-33.e4.
844 29. Brown AR, Martinez M. Ipsilesional Motor Cortex Plasticity Participates in Spontaneous
845 Hindlimb Recovery after Lateral Hemisection of the Thoracic Spinal Cord in the Rat. The Journal of
846 neuroscience : the official journal of the Society for Neuroscience. 2018; 38: 9977-88.
847 30. Sun G, Yang S, Cao G, Wang Q, Hao J, Wen Q, et al. γδ T cells provide the early source of IFN-γ
848 to aggravate lesions in spinal cord injury. The Journal of experimental medicine. 2018; 215: 521-35.

849 31. Zhou K, Zheng Z, Li Y, Han W, Zhang J, Mao Y, et al. TFE3, a potential therapeutic target for
850 Spinal Cord Injury via augmenting autophagy flux and alleviating ER stress. Theranostics. 2020; 10:
851 9280-302.
852 32. Kamens HM, Crabbe JC. The parallel rod floor test: a measure of ataxia in mice. Nature protocols.
853 2007; 2: 277-81.
854 33. Sardina F, Pisciottani A, Ferrara M, Valente D, Casella M, Crescenzi M, et al. Spastin recovery in
855 hereditary spastic paraplegia by preventing neddylation-dependent degradation. Life science alliance.
856 2020; 3.
857 34. Kaplan A, Morquette B, Kroner A, Leong S, Madwar C, Sanz R, et al. Small-Molecule
858 Stabilization of 14-3-3 Protein-Protein Interactions Stimulates Axon Regeneration. Neuron. 2017; 93:
859 1082-93.e5.
860 35. Saponaro A, Porro A, Chaves-Sanjuan A, Nardini M, Rauh O, Thiel G, et al. Fusicoccin Activates
861 KAT1 Channels by Stabilizing Their Interaction with 14-3-3 Proteins. The Plant cell. 2017; 29:
862 2570-80.
863 36. Petosa C, Masters SC, Bankston LA, Pohl J, Wang B, Fu H, et al. 14-3-3zeta binds a
864 phosphorylated Raf peptide and an unphosphorylated peptide via its conserved amphipathic groove.
865 The Journal of biological chemistry. 1998; 273: 16305-10.
866 37. Pisa R, Cupido T, Kapoor TM. Designing Allele-Specific Inhibitors of Spastin, a
867 Microtubule-Severing AAA Protein. Journal of the American Chemical Society. 2019; 141: 5602-6.
868 38. Pisa R, Cupido T, Steinman JB, Jones NH, Kapoor TM. Analyzing Resistance to Design Selective
869 Chemical Inhibitors for AAA Proteins. Cell chemical biology. 2019; 26: 1263-73.e5.
870 39. Savolainen KM, Loikkanen J, Eerikäinen S, Naarala J. Glutamate-stimulated ROS production in
871 neuronal cultures: interactions with lead and the cholinergic system. Neurotoxicology. 1998; 19:
872 669-74.
873 40. Kajiwara Y, Buxbaum JD, Grice DE. SLITRK1 binds 14-3-3 and regulates neurite outgrowth in a
874 phosphorylation-dependent manner. Biological psychiatry. 2009; 66: 918-25.
875 41. Zerr I. Laboratory Diagnosis of Creutzfeldt-Jakob Disease. The New England journal of medicine.
876 2022; 386: 1345-50.
877 42. van den Brand R, Heutschi J, Barraud Q, DiGiovanna J, Bartholdi K, Huerlimann M, et al.

878 Restoring voluntary control of locomotion after paralyzing spinal cord injury. Science (New York, NY).
879 2012; 336: 1182-5.
880 43. Perrin FE, Noristani HN. Serotonergic mechanisms in spinal cord injury. Experimental neurology.
881 2019; 318: 174-91.
882 44. Yuan A, Rao MV, Veeranna, Nixon RA. Neurofilaments and Neurofilament Proteins in Health and
883 Disease. Cold Spring Harbor perspectives in biology. 2017; 9.
884 45. Liu B, Xin W, Tan JR, Zhu RP, Li T, Wang D, et al. Myelin sheath structure and regeneration in
885 peripheral nerve injury repair. Proceedings of the National Academy of Sciences of the United States of
886 America. 2019; 116: 22347-52.
887 46. Ceto S, Sekiguchi KJ, Takashima Y, Nimmerjahn A, Tuszynski MH. Neural Stem Cell Grafts
888 Form Extensive Synaptic Networks that Integrate with Host Circuits after Spinal Cord Injury. Cell stem
889 cell. 2020; 27: 430-40.e5.
890 47. Venkatesh K, Ghosh SK, Mullick M, Manivasagam G, Sen D. Spinal cord injury:
891 pathophysiology, treatment strategies, associated challenges, and future implications. Cell and tissue
892 research. 2019; 377: 125-51.
893 48. Ko SH, Apple EC, Liu Z, Chen L. Age-dependent autophagy induction after injury promotes axon
894 regeneration by limiting NOTCH. Autophagy. 2020; 16: 2052-68.
895 49. Griffin JM, Bradke F. Therapeutic repair for spinal cord injury: combinatory approaches to
896 address a multifaceted problem. EMBO molecular medicine. 2020; 12: e11505.
897 50. Lin YF, Xie Z, Zhou J, Chen HH, Shao WW, Lin HD. Effect of exogenous spastin combined with
898 polyethylene glycol on sciatic nerve injury. Neural regeneration research. 2019; 14: 1271-9.
899 51. Sarbanes SL, Zehr EA, Roll-Mecak A. Microtubule-severing enzymes. Current biology : CB.
900 2022; 32: R992-r7.
901 52. Vemu A, Szczesna E, Zehr EA, Spector JO, Grigorieff N, Deaconescu AM, et al. Severing
902 enzymes amplify microtubule arrays through lattice GTP-tubulin incorporation. Science (New York,
903 NY). 2018; 361.
904 53. Jiang T, Cai Z, Ji Z, Zou J, Liang Z, Zhang G, et al. The lncRNA MALAT1/miR-30/Spastin Axis
905 Regulates Hippocampal Neurite Outgrowth. Frontiers in cellular neuroscience. 2020; 14: 555747.
906 54. Costa AC, Sousa MM. The Role of Spastin in Axon Biology. Frontiers in cell and developmental

907 biology. 2022; 10: 934522.
908 55. Zhang J, Pho V, Bonasera SJ, Holtzman J, Tang AT, Hellmuth J, et al. Essential function of HIPK2
909 in TGFbeta-dependent survival of midbrain dopamine neurons. Nature neuroscience. 2007; 10: 77-86.
910 56. Cornell B, Wachi T, Zhukarev V, Toyo-Oka K. Regulation of neuronal morphogenesis by
911 14-3-3epsilon (Ywhae) via the microtubule binding protein, doublecortin. Human molecular genetics.
912 2016; 25: 4405-18.
913 57. Dar A, Wu D, Lee N, Shibata E, Dutta A. 14-3-3 proteins play a role in the cell cycle by shielding
914 cdt2 from ubiquitin-mediated degradation. Molecular and cellular biology. 2014; 34: 4049-61.
915 58. Lee JH, Lu H. 14-3-3Gamma inhibition of MDMX-mediated p21 turnover independent of p53.
916 The Journal of biological chemistry. 2011; 286: 5136-42.
917 59. Chan TY, Egbert CM, Maxson JE, Siddiqui A, Larsen LJ, Kohler K, et al. TNK1 is a
918 ubiquitin-binding and 14-3-3-regulated kinase that can be targeted to block tumor growth. Nature
919 communications. 2021; 12: 5337.
920 60. Kast DJ, Dominguez R. Mechanism of IRSp53 inhibition by 14-3-3. Nature communications.
921 2019; 10: 483.
922 61. Cornell B, Toyo-Oka K. 14-3-3 Proteins in Brain Development: Neurogenesis, Neuronal
923 Migration and Neuromorphogenesis. Frontiers in molecular neuroscience. 2017; 10: 318.
924 62. Marra M, Camoni L, Visconti S, Fiorillo A, Evidente A. The Surprising Story of Fusicoccin: A
925 Wilt-Inducing Phytotoxin, a Tool in Plant Physiology and a 14-3-3-Targeted Drug. Biomolecules. 2021;
926 11.
927 63. Liu D, Bienkowska J, Petosa C, Collier RJ, Fu H, Liddington R. Crystal structure of the zeta
928 isoform of the 14-3-3 protein. Nature. 1995; 376: 191-4.
929
930

931 **Figures and legends:**

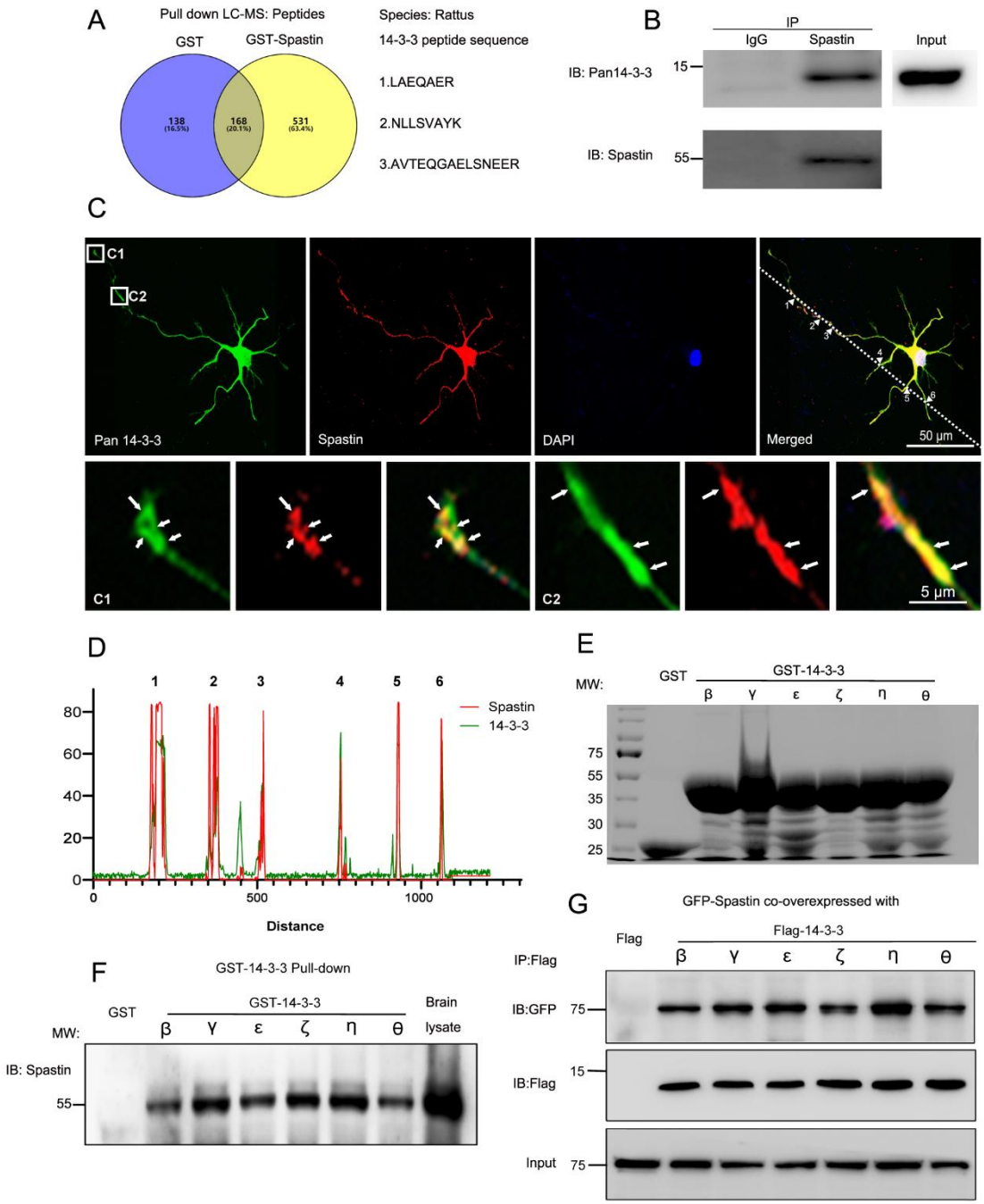

932

933

934 **Figure 1. 14-3-3 physically interacts with spastin in vivo and vitro.** (A) Mass
935 spectrum of peptides which was pull-downed by GST-spastin from proteins of the
936 spinal cord tissue (near 1 cm around the T10 level), the representative peptides of
937 14-3-3 were shown. (B) Immunoprecipitation assay using spastin antibody was
938 performed and Pan 14-3-3 antibody was used for western blotting. (C) Hippocampal

939 neurons were stained with 14-3-3s (green) and spastin (red) antibodies, the growth
940 cone (C1) and axon shaft (C2) profile were shown. (D) Localization of spastin (red
941 line) and 14-3-3 (green line) protein in the hippocampal neurons were analyzed and
942 the intensity of the white dotted line across the neurite compartment were measured.
943 (E) Purified GST and GST-14-3-3s fusion proteins were subjected to sodium
944 dodecyl-sulfate polyacrylamide gel electrophoresis and coomassie blue staining was
945 confirmed the successful purification of relative proteins. (F) GST fusion proteins
946 were used to pull down the lysates of the spinal cord and spastin antibody was used
947 for western blotting. (G) HEK 293T cells were transfected with Flag tagged 14-3-3s
948 and GFP tagged spastin, the cell lysates were subjected to GFP-Trap assay, Flag
949 antibody was used to detect the presence of 14-3-3s.

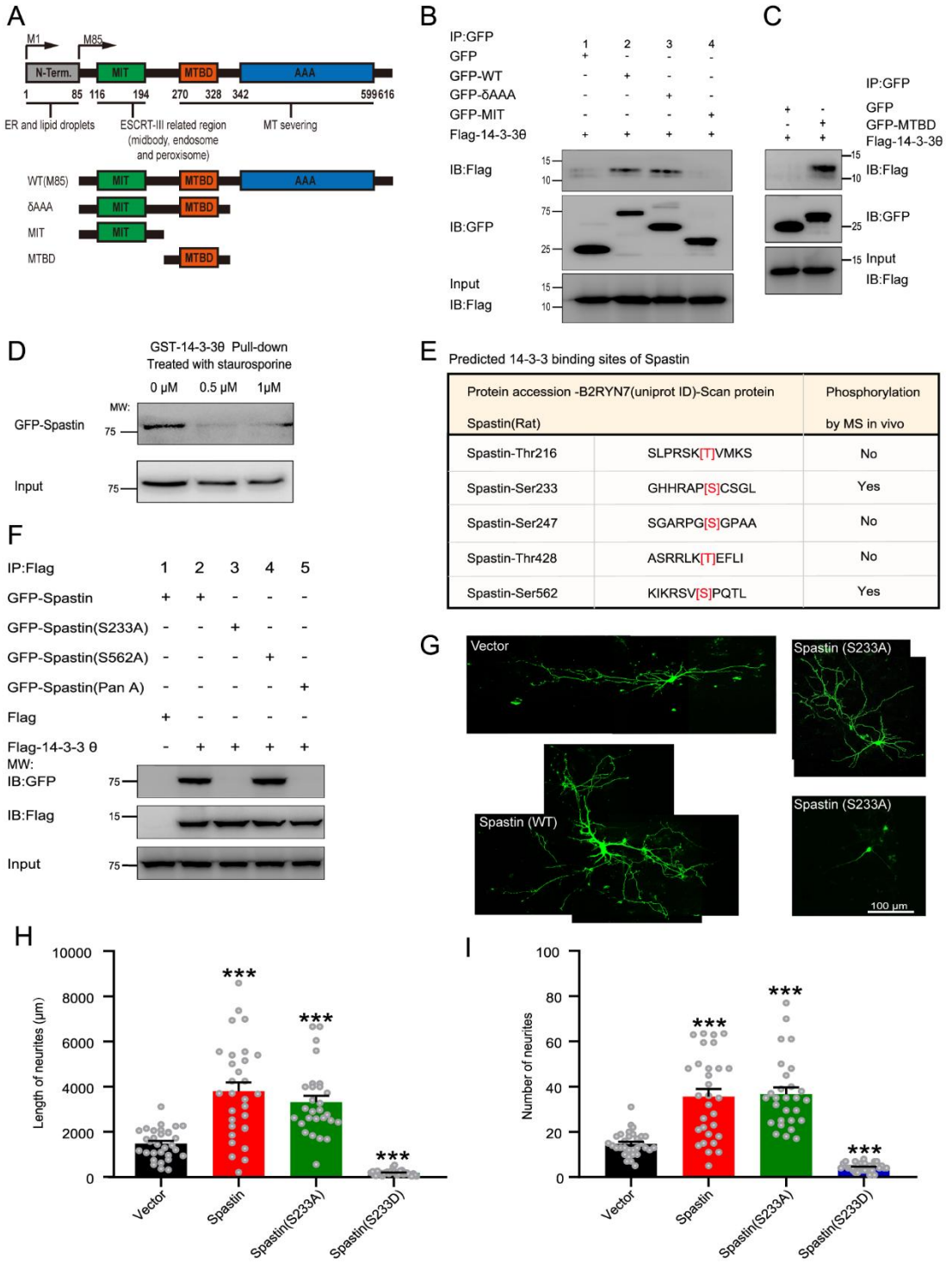

Figure 2. Ser233 in spastin is essential for the interaction with 14-3-3 and important for neurite outgrowth. (A) Schematic illustration of the gene truncation strategy for the modular domain of spastin. (B) Truncation mutants of spastin together with Flag tagged 14-3-3 were transfected into HEK 293T cells, and cell lysates were immunoprecipitated by GFP-Trap assay. Flag antibody were used for detecting the

956 flag tagged 14-3-3 fusion protein. (C) The microtubule binding domain (MTBD)
957 truncated GFP tagged spastin were transfected together with Flag tagged 14-3-3 into
958 HEK 293T cells, and subjected to GFP trap assay. (D) HEK 293T cells were
959 transfected with GFP-spastin and then treated with or without staurosporine for 1 hour.
960 Cell lysates were pull down by GST 14-3-3 fusion protein and GFP antibody were
961 used for western blotting. (E) The binding sites between 14-3-3 and spastin were
962 predicted using the scansite 2.0 software and whether these sites could be
963 phosphorylated were confirmed by phosphosite plus website. (F) Serine 233 and
964 Serine 562 of spastin were mutated to alanine, these GFP fusion mutations were
965 transfected together with Flag tagged 14-3-3, then cell lysates were subjected to
966 GFP-trap assay. Flag antibody was used to detect the binding ability between spastin
967 mutations and 14-3-3. (G) Hippocampal neurons were grown on DIV 2 and
968 transfected with spastin Ser233 mutations (Spastin S233A, Spastin S233D), then fixed
969 on DIV 3. Representative images of transfected neurons as indicated were shown.
970 Quantitative analysis of the length of neurites (H) and the number of neurites (I) were
971 shown (n≥25 per group). All error bars are SEM. *P <0.05. Scale bar: 100 μm.

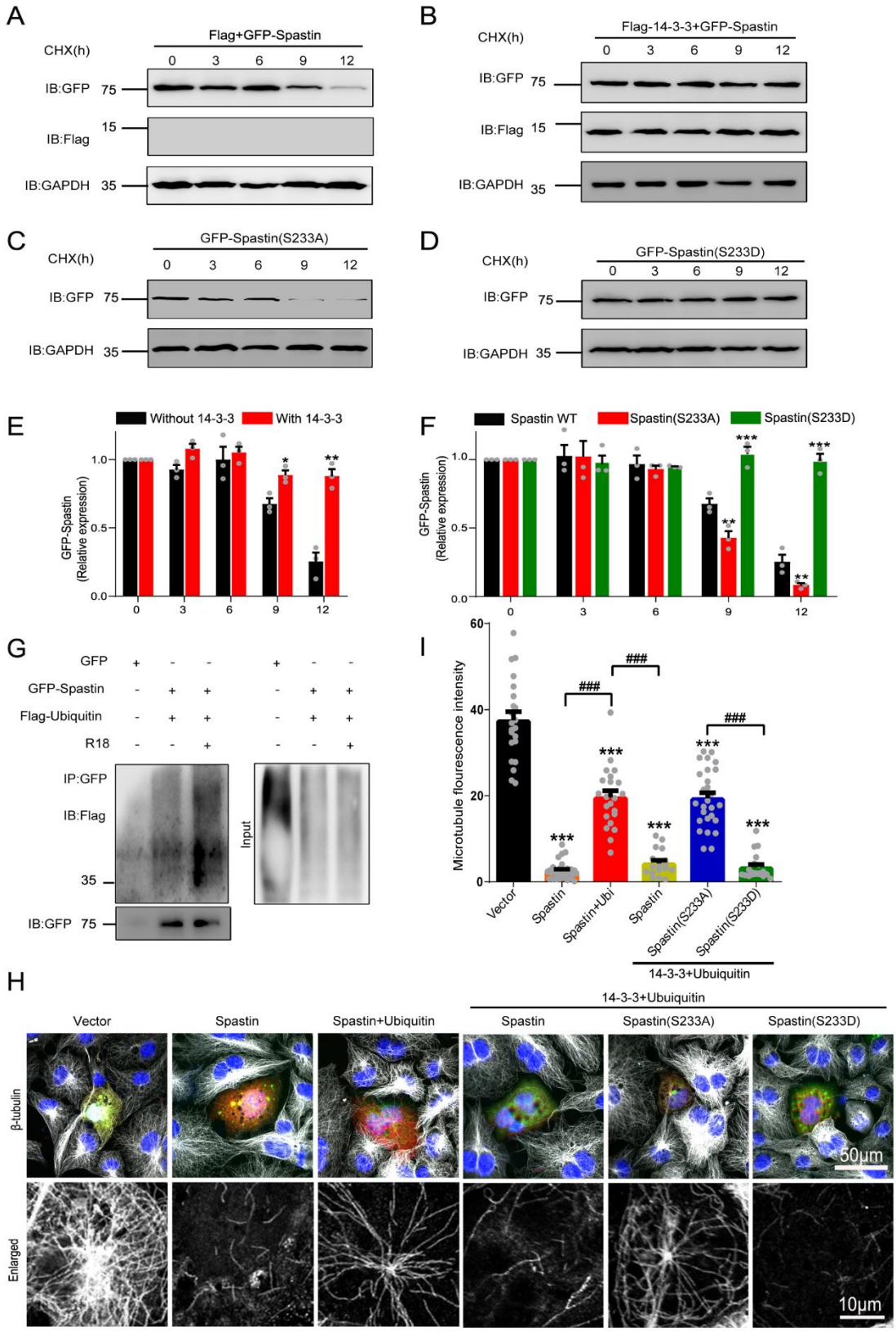

Figure 3. 14-3-3 protein protects spastin by Ser233 phosphorylation from degradation through ubiquitin pathway. (A) GFP tagged spastin together with Flag tagged 14-3-3 (B) or without was transfected into HEK 293T cells. Following the

976 addition of protein synthesis inhibitor (cycloheximide, CHX), cell lysates were
977 subjected to western blot to detect the GFP tagged spastin protein levels. (C, D)
978 Western blot analysis of HEK 293T cell lysates transfected with spastin mutations
979 (S233A or S233D) after treating with cycloheximide at different indicated times. (E)
980 Quantitative analysis of spastin protein levels after treating by cycloheximide with or
981 without 14-3-3 protein. (F) Quantitative analysis of GFP tagged spastin protein levels
982 upon transfected with different spastin mutations. (G) HEK 293T cells were
983 transfected with GFP tagged spastin and Flag tagged ubiquitin, together with R18 or
984 not, cells were harvested and subjected to immunoprecipitation using GFP antibody.
985 Flag antibody was used to detect the ubiquitin band. (H) COS7 cells were transfected
986 with indicated GFP tagged spastin with or without Flag tagged ubiquitin for 24 hours.
987 Then, cells were fixed and stained with tubulin antibody to visualize microtubule
988 arrangements. (I) The normalized quantitative analysis of microtubule fluorescence
989 intensity among indicated groups (n≥20 pictures per group). *$P < 0.05$, **$P < 0.01$,
990 ***$P < 0.001$. Scale bar: 50 μm, 10 μm.

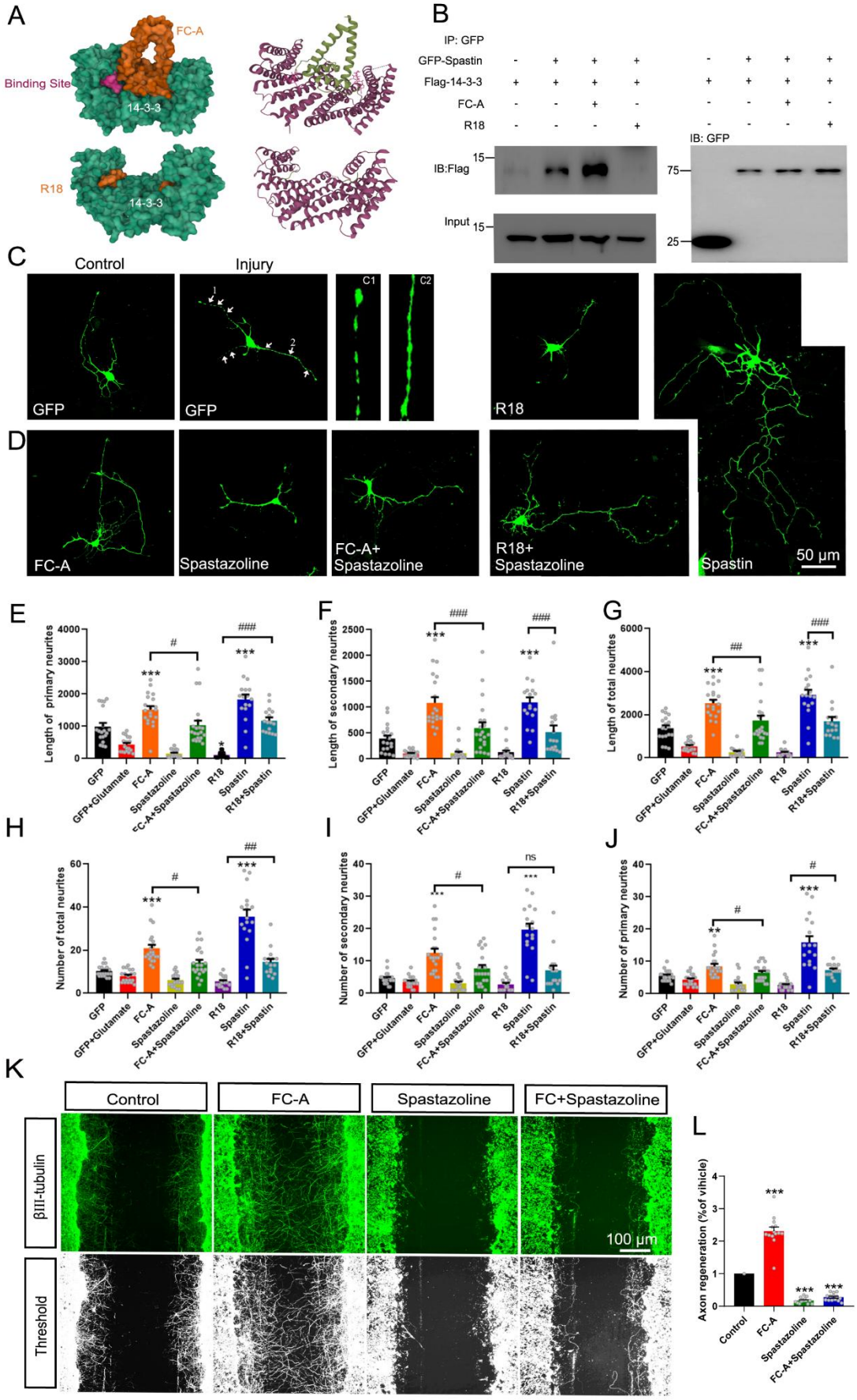
A
FC-A
Binding Site
14-3-3
R18
14-3-3
B
IP: GFP
GFP-Spastin
Flag-14-3-3
FC-A
R18
IB:Flag
Input
IB: GFP
C
Control
Injury
GFP
GFP
C1
C2
R18
D
FC-A
Spastazoline
FC-A+ Spastazoline
R18+ Spastazoline
Spastin
50 μm
E
Length of primary neurites
F
Length of secondary neurites
G
Length of total neurites
H
Number of total neurites
I
Number of secondary neurites
J
Number of primary neurites
GFP
GFP+Glutamate
FC-A
Spastazoline
FC-A+Spastazoline
R18
Spastin
R18+Spastin
K
Control
FC-A
Spastazoline
FC+Spastazoline
βIII-tubulin
Threshold
100 μm
L
Axon regeneration (%of vihicle)
Control
FC-A
Spastazoline
FC-A+Spastazoline

991

992

Figure 4. 14-3-3 agonist Fusicoccin (FC-A) promotes the repair of neurite outgrowth and regeneration after injury via spastin. (A) The surface structure and (B) secondary structure of molecular docking model between 14-3-3 protein with FC-A (PDB:2O98) or R18 (PDB:1A38). (C) HEK 293T cells were transfected with GFP tagged spastin and Flag tagged 14-3-3, cell lysates were incubated with FC-A or R18 and then subjected to GFP-trap assay. Flag antibody were used to detect the 14-3-3 binding. (C) Hippocampal neurons (DIV2) were transfected with GFP to visualize its morphology. Neurons were then incubated with glutamate (120 μM) to induce injury, the neurite breakages and swellings were found in C1 and C2. (D) The injured neurons were transfected with spastin and incubated with FC-A, R18 or spastazoline for 24 hours, then cells were fixed and images were taken by confocal microscopy. Neurons were traced using Image J Pro Plus and quantitative analysis of the length of primary neurites (E), secondary neurites (F) and total neurites (G) were performed. Quantitative analysis of the number of primary neurites (H), secondary neurites (I) and total neurites (J). $^{*}P < 0.05$, $^{**}P < 0.01$, $^{***}P < 0.001$. Scale bar: 50 μm. (K) Primary cortical neurons were grown and scratch assays were performed at DIV7. FC-A or spastazoline were applied and incubated for 36 hours. Then, cells were stained with βIII-tubulin to visualize the morphology of neurites. (L) Quantitative analysis of the normalized axon regeneration rate. $^{*}P < 0.05$, $^{**}P < 0.01$, $^{***}P < 0.001$. Scale bar: 100 μm.

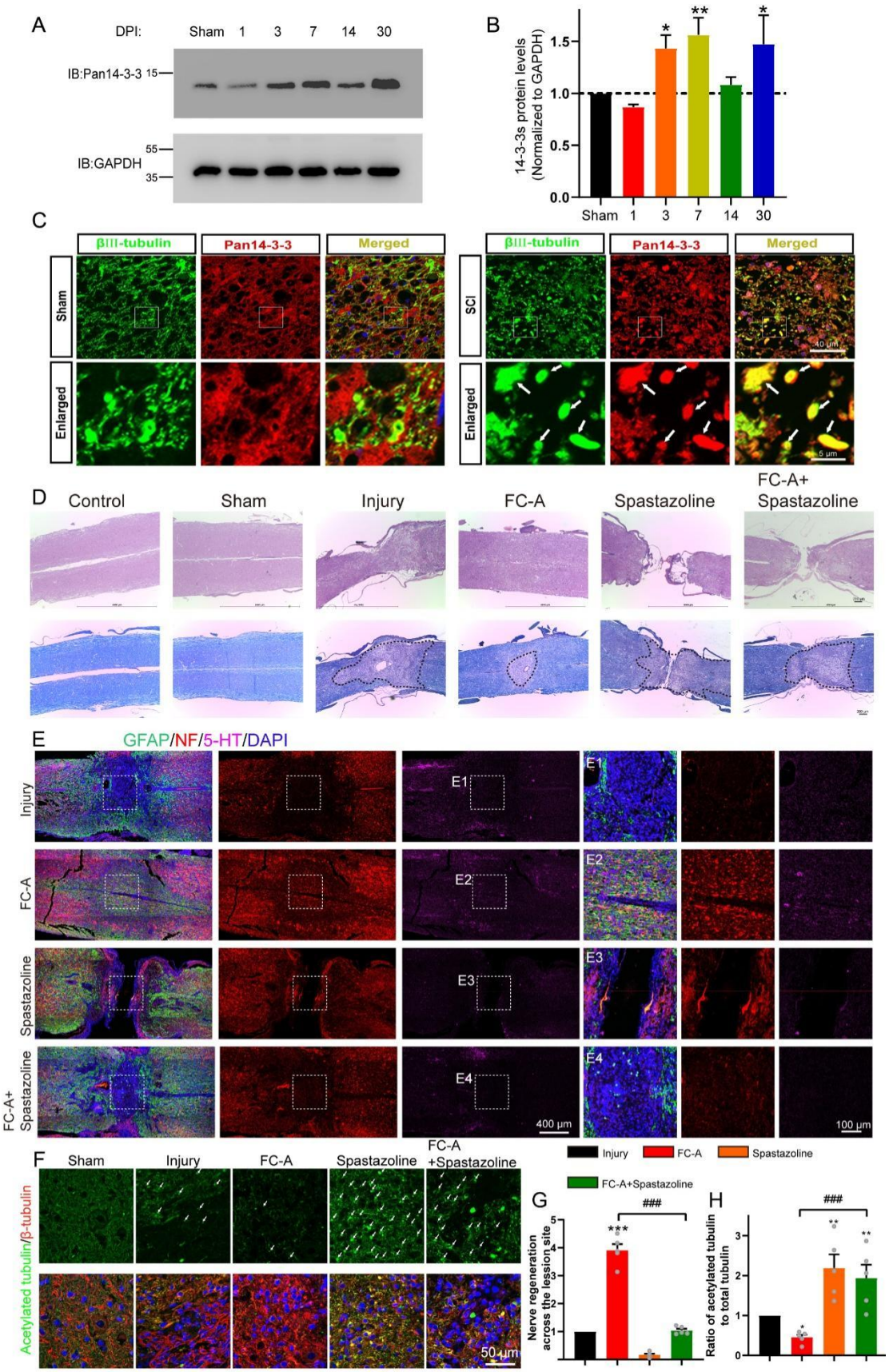
A
DPI:
Sham 1 3 7 14 30
IB:Pan14-3-3 15
IB:GAPDH
55
35
B
14-3-3s protein levels (Normalized to GAPDH)
1.5
1.0
0.5
0.0
Sham 1 3 7 14 30
C
βIII-tubulin
Pan14-3-3
Merged
Sham
SCI
Enlarged
40 μm
5 μm
D
Control
Sham
Injury
FC-A
Spastazoline
FC-A+ Spastazoline
E
GFAP/NF/5-HT/DAPI
Injury
FC-A
Spastazoline
FC-A+ Spastazoline
E1
E2
E3
E4
400 μm
100 μm
F
Sham
Injury
FC-A
Spastazoline
FC-A +Spastazoline
Acetylated tubulin/β-tubulin
50 μm
Injury
FC-A
Spastazoline
FC-A+Spastazoline
G
Nerve regeneration across the lesion site
###
***
H
Ratio of acetylated tubulin to total tubulin
###
**

1013

1014

Figure 5. 14-3-3/spastin pathway is involved in nerve regeneration after spinal cord injury by targeting MTs. (A) After spinal cord contusion, the spinal cord tissues of the lesion site (near 1 cm) at indicated times (1, 3, 7 14, and 30 DPI) were ground and lysed, then subjected to western blot. (B) Quantitative analysis of the 14-3-3 protein expression (n=3 per group). (C) The lesion site of spinal tissue in the sham group and the SCI group were stained with Pan 14-3-3 (red) and β III tubulin (green). The arrows mean the elevated 14-3-3 protein in the neuronal compartment. (D) 14-3-3 agnoist FC-A and spastin inhibitor spastazoline were admisnistrated after spinal cord contusion. At 45 DPI (Days post-injury), the tissues were fixed and embedded, then cut horizontally and longitudinally. H&E and LFB (Luxol fast blue stain) were stained. The spinal cord demyelination was shown inside the area of the dotted line. Scale bar， 200 μm. (E) The slices were then subjected to immunofluorescence staining, and GFAP (green) was stained to label astrocytes, NF (red) was stained to label neurons and 5-HT (magenta) was stained to label monoaminergic axons. The lesion site in different groups was boxed and enlarged in (E1)(E2)(E3)(E4). Scale bar, 400 μm, and 100 μm. (F) The spinal cord slices were stained with acetylated tubulin (Stable MTs which lack of dynamics) and β-tubulin (total tubulin). Scale bar，50 μm. (G) The normalized intensity of NF was quantified (n=5 animals per group). Mean ± SEM. $*P < 0.05$, $**P < 0.01$, $***P < 0.001$. (H) The normalized ratio of acetylation tubulin to total tubulin was calculated by the intensity value of acetylated tubulin divided by total tubulin (n=5 pictures per group). Mean ± SEM. $*P < 0.05$, $**P < 0.01$, $***P < 0.001$.

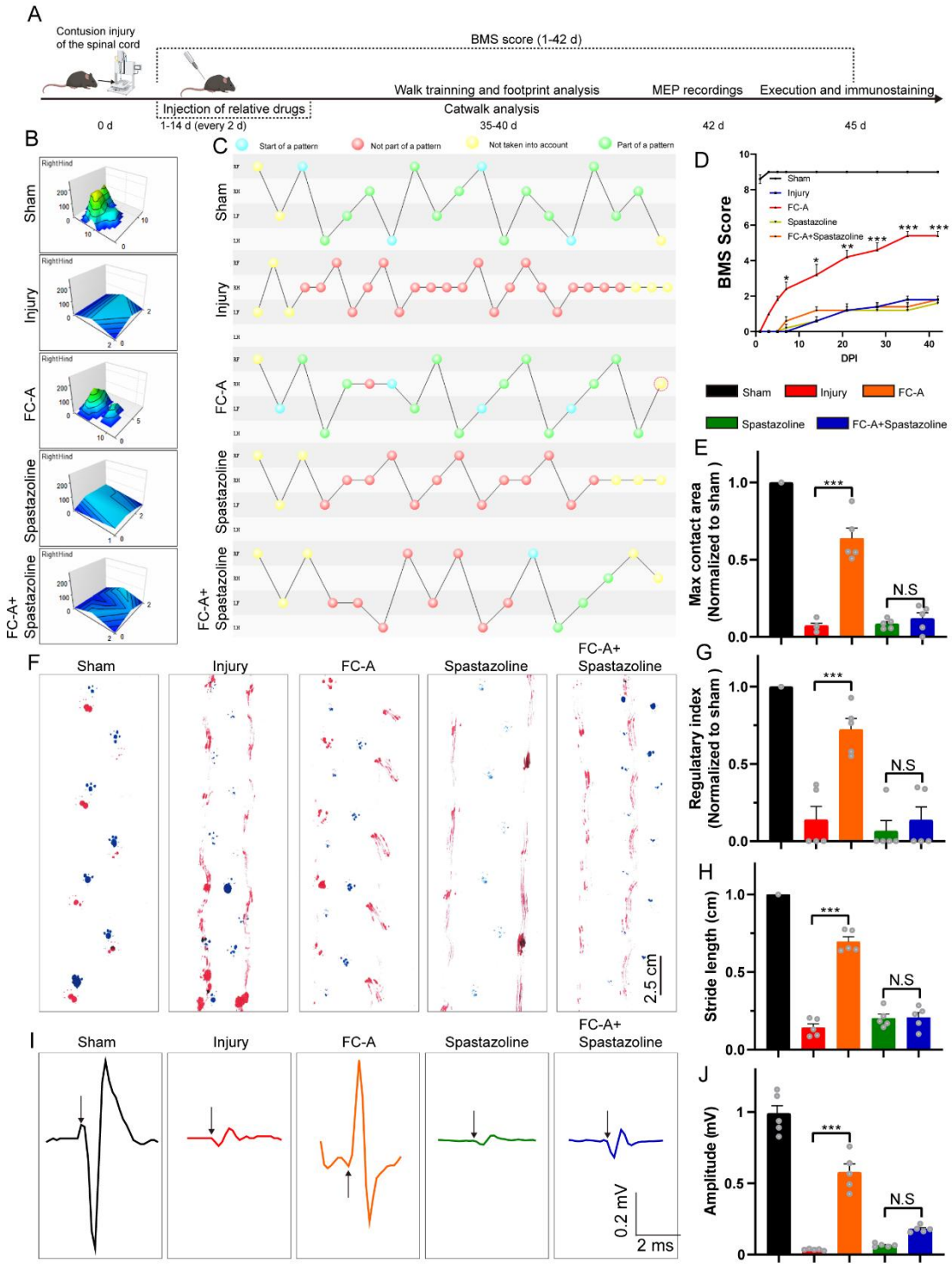

Figure 6. 14-3-3/spastin pathway coordinates locomotor recovery after spinal cord contusion. (A) Schematic illustration of relative treatments and examinations at different indicated times. (B) The max contact areas of the right hindlimb were recorded and analyzed by the Catwalk software. (C) The footfall patterns were visualized by the Catwalk software. The blue dot represents the start of a pattern. The

1043 red dot represents the gait was not part of a pattern. The yellow dot represents that the
1044 gait was not taken into account. The green one means the gait belongs to a normal
1045 part of a pattern. (D) BMS score at different indicated days after injury and data were
1046 represented as mean±SEM. (n=5 group, data were analyzed by one way ANOVA and
1047 Bonferroni's multiple-comparison test were used for post hoc comparisons. (E) The
1048 quantitative analysis of the hindlimb (right) max contact area. (n=5 animals per
1049 group). (F) Footprint analysis of the mice at 6 weeks after spinal cord contusion.
1050 The forelimbs were marked with blue and the hindlimbs were marked with red. Scale
1051 bar: 2.5 cm. (G) The normalized regularity index of the footfall pattern calculated by
1052 Catwalk software (~100 % in the sham group, n=5 animals per group). (H)
1053 Quantatitive analysis of the stride length in the footprint assay. The mean stride length
1054 of each walk was counted, n=5 animals per group). (I) Motor evoked potentials
1055 (MEPs) were recorded at 7 weeks after spinal cord contusion. The craniotomy was
1056 performed and the M1 region of the sensorimotor cortex were stimulated by single
1057 square-wave stimulus of 0.5 mA, 0.5 ms duration, 2 ms time delay, and 1 Hz. The
1058 MEP were recorded with the signals detected by the electrode on the gastrocnemius
1059 muscle. The representative histograms of the amplitude-times are shown. The arrows
1060 indicated the stimulus. (J) The current amplitudes of the MEP were quantified, n=5
1061 animals per group. Mean ± SEM. *$P < 0.05$, **$P < 0.01$, ***$P < 0.001$.

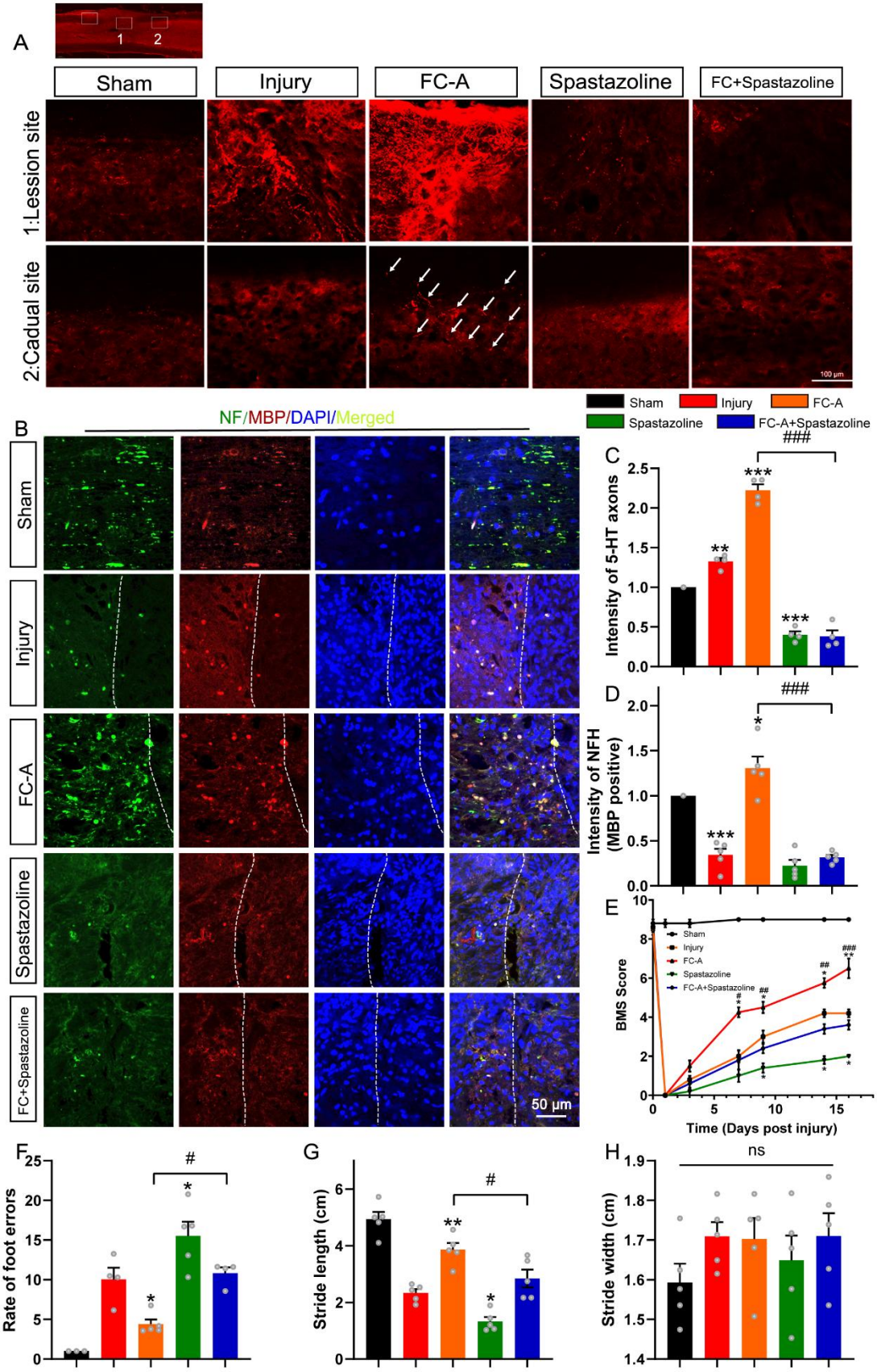
A
1
2
Sham
Injury
FC-A
Spastazoline
FC+Spastazoline
1:Lession site
2:Cadual site
100 μm
Sham
Injury
FC-A
Spastazoline
FC-A+Spastazoline
B
NF/MBP/DAPI/Merged
Sham
Injury
FC-A
Spastazoline
FC+Spastazoline
50 μm
C
Intensity of 5-HT axons
D
Intensity of NFH (MBP positive)
E
BMS Score
Time (Days post injury)
F
Rate of foot errors
G
Stride length (cm)
H
Stride width (cm)
ns

1062

1063

1064 **Figure 7. FC-A promotes axon regeneration in a T10 lateral hemisection spinal**
1065 **cord injury model.** (A) The spinal cords of adult mice were subjected to lateral
1066 hemisection and administrated by intraperitoneal injection with FC-A or spastazoline.
1067 Sagittal view of 5-HT-immunoreactive raphespinal fibers in the spinal cord on 17 DPI.
1068 Scale bar, 500 μm and 100 μm. (B) Sagittal view of neurofilaments which was MBP
1069 positive in the white manner of the lesion site of the spinal cord. Scale bar, 50 μm. (C)
1070 The normalized quantification of 5-HT immunoreactive fluorescence intensity (0.5
1071 mm caudal to the lesion site, n=5 animals per group). (D) The normalized
1072 quantification of NF (Neurofilament) immunoreactive fluorescence intensity in the
1073 lesion site (n=5 animals per group). (E) The locomotor function of mice after SCI
1074 were scored at the indicated time points according to the standard of Basso Mouse
1075 Scale (BMS). (F) Foot fault test was performed and the total steps and steps drop out
1076 of the right hindlimb were recorded. The rate of the foot errors was analyzed, n=5
1077 animals per group. *$P < 0.05$, **$P < 0.01$, ***$P < 0.001$. (G) (H)The footprint assay
1078 was performed and stride length (G) and stride width (H) quantitative analyzed. Data
1079 were presented as mean ± SEM, n=5 animals per group, the mean value of each
1080 animal' s walk were calculated.
1081
1082
1083